

1 **Climate change increases riverine carbon outgassing while export to**  
2 **the ocean remains uncertain**

3

4 F. Langerwisch<sup>1,2</sup>, A. Walz<sup>3</sup>, A. Rammig<sup>1,4</sup>, B. Tietjen<sup>5,2</sup>, K. Thonicke<sup>1,2</sup>, W. Cramer<sup>6,2</sup>

5 <sup>1</sup> Earth System Analysis, Potsdam Institute for Climate Impact Research (PIK), P.O. Box 60 12  
6 03, Telegraphenberg A62, D-14412 Potsdam, Germany

7 <sup>2</sup> Berlin-Brandenburg Institute of Advanced Biodiversity Research (BBIB), 14195 Berlin,  
8 Germany

9 <sup>3</sup> Institute of Earth and Environmental Science, University of Potsdam, Karl-Liebknecht-Str. 24-  
10 25, D-14476 Potsdam-Golm, Germany

11 <sup>4</sup>TUM School of Life Sciences Weihenstephan, Land Surface-Atmosphere Interactions,  
12 Technical University Munich, Hans-Carl-von-Carlowitz-Platz 2, 85354 Freising, Germany

13 <sup>5</sup> Biodiversity – Ecological Modelling, Institute of Biology, Freie Universität Berlin,  
14 Altensteinstr. 6, D-14195 Berlin, Germany

15 <sup>6</sup> Institut Méditerranéen de Biodiversité et d'Ecologie marine et continentale (IMBE), Aix  
16 Marseille Université, CNRS, IRD, Avignon Université, Technopôle Arbois-Méditerranée, Bât.  
17 Villemin - BP 80, F-13545 Aix-en-Provence cedex 04, France

18

19 *Correspondence to:* F. Langerwisch (langerwisch@pik-potsdam.de)

20

21        **Abstract**

22    Any regular interaction of land and river during flooding affects carbon pools within the  
23    terrestrial system, riverine carbon, and carbon exported from the system. In the Amazon basin  
24    carbon fluxes are considerably influenced by annual flooding during which terrigenous organic  
25    material is imported to the river. The Amazon basin represents therefore an excellent example of  
26    a tightly coupled terrestrial-riverine system. The processes of generation, conversion, and  
27    transport of organic carbon in such a coupled terrigenous-riverine system strongly interact and  
28    are climate-sensitive, yet their functioning is rarely considered in Earth system models and their  
29    response to climate change is still largely unknown. To quantify regional and global carbon  
30    budgets and climate change effects on carbon pools and carbon fluxes it is important to account  
31    for the coupling between the land, the river, the ocean and the atmosphere. We developed the  
32    riverine carbon model RivCM, which is directly coupled to the well-established dynamic  
33    vegetation and hydrology model LPJmL in order to account for this large scale coupling. We  
34    evaluate RivCM with observational data and show that some of the values are reproduced quite  
35    well by the model while we see large deviations for other variables. This is mainly caused by  
36    some simplifications we assumed. Our evaluation shows that it is possible to reproduce large  
37    scale carbon transport across a river system however with large uncertainties. Acknowledging  
38    these uncertainties, we estimate the potential changes in riverine carbon by applying RivCM for  
39    climate forcing from five climate models and three CO<sub>2</sub> emission scenarios (SRES). We find that  
40    climate change causes a doubling of riverine organic carbon in the Southern and Western basin  
41    while reducing it by 20% in the Eastern and Northern parts. In contrast, the amount of riverine  
42    inorganic carbon shows a 2- to 3-fold increase in the entire basin, independent of the SRES  
43    scenario. The export of carbon to the atmosphere increases as well with an average of about  
44    30%. In contrast, changes in future export of organic carbon to the Atlantic Ocean depend on the  
45    SRES scenario and are projected to either decrease by about 8.9% (SRES A1B) or increase by  
46    about 9.1% (SRES A2). Such changes in the terrigenous-riverine system could have local and  
47    regional impacts on the carbon budget of the whole Amazon basin and parts of the Atlantic  
48    Ocean. Changes in the riverine carbon could lead to a shift in the riverine nutrient supply and  
49    pH, while changes in the exported carbon to the ocean leads to changes in the supply of organic  
50    material that acts as a food source in the Atlantic. At larger scales the increased outgassing of  
51    CO<sub>2</sub> could turn the Amazon basin from a sink of carbon to a considerable source. Therefore we  
52    propose that the coupling of terrestrial and riverine carbon budget should be included in  
53    subsequent analysis of the future regional carbon budget.

54

## 55 1 Introduction

56 Research on the effects of climate and land use change on terrestrial and riverine systems has  
57 been extensively conducted. Results show how changes in temperature and precipitation will  
58 affect the species composition in forest ecosystems (Fearnside, 2004; Huntingford et al., 2013;  
59 Nepstad et al., 2007) as well as discharge and flooding patterns of rivers (Coe et al., 2011;  
60 Panday et al., 2015; Zulkafli et al., 2016). However, the consequences for a coupled terrestrial-  
61 riverine system have been elaborated on in less detail and mostly focusing on estimations under  
62 the current climate (Johnson et al., 2006; Cole et al., 2000; Richey et al., 2002; Neu et al., 2011;  
63 Abril et al., 2014). Here we want to deepen the understanding of consequences of climate change  
64 on riverine carbon fluxes, which are fuelled by vegetation, and on the export of carbon from the  
65 terrestrial part to the atmosphere and the ocean. We aim to understand how much the basin-wide  
66 carbon balance is influenced by these interactions.

67 In this study we focus on the coupled terrestrial-riverine system on the Amazon basin. In this  
68 region the Amazon River and in particular, the annually recurring flooding of parts of the forests,  
69 shape the manifold Amazonian ecosystems. The flooding is most decisive for the coupling of  
70 terrestrial and aquatic processes by transferring organic material from the terrestrial ecosystems  
71 in the river (Hedges et al., 2000). The water rises with an amplitude of only some centimetres in  
72 small tributaries to up to 15 meters in the main stem (Junk, 1985). In central Amazonia about  
73 16% of the area is flooded during high water, while only 4% are flooded permanently (Richey et  
74 al., 2002). During flooding, deposited litter and soil carbon which originates from terrestrial  
75 vegetation is one source of organic material imported into the river system. The input of  
76 terrigenous organic material affects the riverine system enormously on a local scale (Melack and  
77 Forsberg, 2001; Waterloo et al., 2006). It acts, for instance, as fertilizer and food source  
78 (Anderson et al., 2011; Horn et al., 2011), and is a modifier of habitats and interacting local  
79 carbon cycles (Hedges et al., 2000; Irmiler, 1982; Johnson et al., 2006; McClain and Elsenbeer,  
80 2001). Whereas in most limnic systems additional organic material produced by aquatic  
81 photosynthesis plays a major role for the riverine organic carbon pools (Lampert and Sommer,  
82 1999; Schwoerbel and Brendelberger, 2005), the aquatic photosynthesis rate in large parts of the  
83 Amazon River network is comparably low and submerged plants rarely occur (Junk and Piedade,  
84 1997). Here, the input of allochthonous material produced in the floodplain forests is more  
85 relevant than the production of organic matter within the river (Abril et al., 2014; Cole and  
86 Caraco, 2001; Druffel et al., 2005; Mayorga et al., 2005). The low aquatic productivity in the  
87 river system is caused by high sediment load and thus high turbidity in white water rivers and  
88 low nutrient supply in the black water rivers (Benner et al., 1995; Richey et al., 1990; Sioli,  
89 1957).

90 At larger scales, the release of carbon into the atmosphere and the export to the ocean are the  
91 most relevant factors, when it comes to estimating the effects of Amazon ecosystems on climate  
92 change. Approximately  $32.7 \times 10^{12}$  g C yr<sup>-1</sup> (Moreira-Turcq et al., 2003) of total organic carbon

93 (TOC) is exported to the Atlantic Ocean, in comparison to about  $470 \times 10^{12}$  g C yr<sup>-1</sup> (Richey et  
94 al., 2002) exported to the atmosphere as CO<sub>2</sub>. While the carbon released to the atmosphere  
95 proliferates climate change immediately, the carbon exported to the ocean affects the marine  
96 ecosystems over hundreds of square kilometres off the mouth of the Amazon River, thereby  
97 possibly influencing ocean-atmosphere carbon exchange over several weeks to months (Cooley  
98 et al., 2007; Cooley and Yager, 2006; Körtzinger, 2003; Subramaniam et al., 2008).

99 Hydrologic or limnic production as well as transformation and export of carbon have been  
100 estimated in a number of empirical (case) studies. These studies highlight different aspects of the  
101 system, e.g. showing that the carbon within the river mainly originates from tree leaves and other  
102 non-woody material from *Várzea* systems (Hedges et al., 2000; Moreira-Turcq et al., 2003),  
103 describing reasons for temporal and spatial differentiations of organic matter within the river  
104 (Aufdenkampe et al., 2007; Devol et al., 1995), and modelling the hydrological and biochemical  
105 aquatic carbon budget over a 2000-km-reach (Bustillo et al. (2011)). Several studies already  
106 combined the aquatic and the terrestrial compartment of the system by including the adjacent  
107 forests (Johnson et al., 2006; Cole et al., 2000; Richey et al., 2002; Neu et al., 2011; Abril et al.,  
108 2014), but these studies focus on estimating carbon budgets under current climate conditions.

109 By improving the understanding of how future climate change could influence the largest  
110 interconnected ecosystem on Earth (Bauer et al., 2013; Sjögersten et al., 2014), an in-depth  
111 analysis of the coupled terrigenous-riverine carbon fluxes and pools in the Amazon basin is  
112 required. Climate and atmospheric CO<sub>2</sub>, terrestrial productivity, water discharge and flooding  
113 patterns strongly interact and thus control the amount of carbon in the Amazon river. But they  
114 also influence its further conversion and transport within the river system, which finally  
115 determine carbon export to either atmosphere or ocean. This tight coupling of the terrigenous-  
116 riverine system makes the Amazon basin highly sensitive for climate change impacts.

117 This study aims at taking first steps towards an understanding of carbon fluxes in a terrigenous-  
118 river-ocean system under future climate change by addressing the following research questions  
119 for the example of the Amazon basin :

- 120 1) How will the highly interdependent and strongly climate-controlled carbon fluxes and  
121 pools in the Amazon basin change during the 21<sup>st</sup> century?
- 122 2) Which regions in the Amazon basin are likely to be most strongly impacted by climate  
123 change?
- 124 3) How does climate change alter the proportion of carbon immediately released to the  
125 atmosphere vs. carbon exported to the ocean?
- 126 4) How relevant is the amount of riverine outgassed carbon for the basin-wide carbon  
127 budget in a changing climate?

128 To address these questions we developed the **Riverine Carbon Model (RivCM)** and applied it to  
129 the Amazon Basin. RivCM is directly coupled to the dynamic vegetation and hydrology model  
130 LPJmL (Bondeau et al., 2007; Gerten et al., 2004; Rost et al., 2008; Sitch et al., 2003). The

131 riverine carbon model focuses on the export, transport and conversion of terrestrial fixed carbon.  
132 Carbon pools and fluxes for the most important transport and transformation processes are  
133 validated for current conditions based on observational data from the Amazon basin.

134 To investigate potential future changes in the different carbon fluxes and pools, the model was  
135 forced by climate change scenarios that cover a large range of uncertainty in climate change  
136 projections for the Amazon basin. Based on these simulations, we identify areas most heavily  
137 affected by climate change. We estimated temporal changes in the different carbon fluxes and  
138 pools, as well as the carbon released to the atmosphere and exported to the ocean. To  
139 additionally assess the benefit of including inundated areas in the model, a full factorial  
140 experiment was conducted. Herewith the study aims to develop a concept to assess changes in  
141 coupled terrestrial-riverine systems, which is a prerequisite to better quantify regional and global  
142 carbon budgets and consequences of climate change.

143

## 144 **2 Methods**

145 The **Riverine Carbon Model (RivCM)** is a grid-based model simulating riverine carbon  
146 dynamics on monthly time steps. It is coupled to the process-based dynamic global vegetation  
147 and hydrology model LPJmL (Bondeau et al., 2007; Gerten et al., 2004; Rost et al., 2008; Sitch  
148 et al., 2003). RivCM is driven by current and future climate and atmospheric CO<sub>2</sub> data. An  
149 overview about the interconnection between the models and scenarios is given in Fig. 1.

### 150 **2.1 Model descriptions**

#### 151 **2.1.1 The dynamic global vegetation and hydrology model LPJmL**

152 The process-based dynamic global vegetation and hydrology model LPJmL (Bondeau et al.,  
153 2007; Gerten et al., 2004; Rost et al., 2008; Sitch et al., 2003) calculates carbon and  
154 corresponding water fluxes globally with a spatial resolution of  $0.5 \times 0.5$  degree (lat/lon) and  
155 daily time steps. For the simulation of potential natural vegetation and the main processes  
156 controlling its dynamics, LPJmL uses climate data (temperature, precipitation and cloud cover),  
157 atmospheric CO<sub>2</sub>, and soil texture as input. The main processes are photosynthesis based on  
158 Farquhar et al. (1980) and Collatz et al. (1992), auto- and heterotrophic respiration,  
159 establishment, mortality and phenology. These processes lead to dynamic changes in carbon  
160 stored in the vegetation, litter and soil. Simulated water fluxes include evaporation, soil moisture,  
161 snowmelt, runoff, discharge, interception and transpiration. Globally, LPJmL calculates the  
162 performance of nine plant functional types in each grid cell, each of these representing an  
163 assortment of species classified as being functionally similar. In the Amazon basin, LPJmL  
164 primarily simulates three of these plant functional types, representing tropical evergreen and

165 deciduous forest and C4 grasses. The monthly aggregated amounts of carbon stored in litter and  
166 soil, as well as the grid-cell's amount of discharged and stored water are used as an input to  
167 RivCM.

168 LPJmL has been shown to reproduce current patterns of biomass production, river discharge, and  
169 carbon emission through fire, also including managed land (Biemans et al., 2009; Bondeau et al.,  
170 2007; Cramer et al., 2001; Fader et al., 2010; Gerten et al., 2004, 2008; Poulter et al., 2009a;  
171 Rost et al., 2008; Sitch et al., 2003; Thonicke et al., 2010; Wagner et al., 2003). The observed  
172 patterns in water fluxes, such as soil moisture, evapotranspiration, and runoff, are comparable to  
173 stand-alone global hydrological models (Wagner et al., 2003; Gerten et al., 2004; Gordon et al.,  
174 2004; Gerten et al., 2008; Biemans et al., 2009). Several studies on Amazonia have been  
175 conducted showing the effect of climate change on NPP (Poulter et al., 2009b), on carbon stocks  
176 (Gumpenberger et al., 2010), on the risk for forest dieback (Rammig et al., 2010) and also on  
177 riverine related changes such as inundation patterns (Langerwisch et al., 2013; Zulkafli et al.,  
178 2016). The ability of the model to realistically reproduce both, terrestrial carbon and water fluxes  
179 and pools, makes it an excellent tool to investigate the coupling of the terrestrial and riverine  
180 carbon in the Amazon basin.

### 181 **2.1.2 The riverine carbon model RivCM**

182 RivCM is a process-based model which simulates the most important processes impacting  
183 different riverine carbon pools, namely import, conversion and export (see overview in Fig. 2).  
184 The model calculates the four major ecological processes related to the riverine carbon budget of  
185 the Amazon River: mobilization of terrigenous organic material (litter and soil carbon),  
186 (mechanical) decomposition of terrigenous organic material, (biochemical) respiration of  
187 terrigenous organic material, and outgassing of CO<sub>2</sub> to the atmosphere. These processes directly  
188 control the most relevant riverine carbon pools, specifically particulate organic carbon (POC),  
189 dissolved organic carbon (DOC), and inorganic carbon (IC), as well as outgassed carbon  
190 (representing CO<sub>2</sub>), and exported riverine carbon to the ocean (POC, DOC and IC). Since  
191 RivCM is developed to simulate the fate of terrigenous carbon, it neglects the autochthonous  
192 production of organic material within the river. A description of the model including sensitivity  
193 analysis and parameterization can be found in the following and in the Supplementary  
194 Information (SI).

195 The Amazon River mobilizes large amounts of terrigenous organic material from seasonally  
196 flooded forests (*Litc* and *Soilc* in Fig. 2), where dead leaves and twigs are exported to the river  
197 (Irmler, 1982; Wantzen et al., 2008). Given the high productivity in Amazonian forests, this  
198 mobilization considerably increases the amount of organic material in the water (Junk, 1985;  
199 Cole and Caraco, 2001; Junk and Wantzen, 2004). Johnson et al. (2006) and Cole et al. (2000)  
200 showed that terrestrially fixed carbon from the floodplain forests is the major source of respired  
201 organic matter within the river and lakes. In RivCM the *mobilization* process is presented by a  
202 function that calculates the amount of mobilized terrestrially fixed carbon in currently inundated

203 areas (*POC* and *DOC* in Fig. 2) depending on the amount of available exportable terrestrial  
204 organic carbon from dead matter. The monthly inundated area is calculated using current  
205 discharge and discharge from the reference period 1971-2000 and potentially floodable area  
206 (Langerwisch et al., 2013).

207 Another source of organic matter for the river is, besides the import of terrigenous material, the  
208 allochthonous production. In most limnic systems the production of organic material by  
209 photosynthesis by aquatic plants plays a major role in the organic carbon pool (Lampert and  
210 Sommer, 1999; Schwoerbel and Brendelberger, 2005). In Amazonia, however, the aquatic  
211 photosynthesis rate in large parts of the Amazon River network is comparably low and  
212 submerged plants rarely occur (Junk and Piedade, 1997) since the white water rivers contain  
213 large amounts of sediments and are thus turbid and the black water rivers contain only little  
214 nutrients (Benner et al., 1995; Richey et al., 1990; Sioli, 1957). Therefore, the input of  
215 allochthonous material produced in floodplain forests contributes much stronger to total organic  
216 matter within the river than the production by aquatic plants (Cole and Caraco, 2001; Junk, 1985;  
217 Junk and Wantzen, 2004). Therefore, the Amazon river itself is considered rather a transport  
218 agent than a producer of organic material (Junk and Wantzen, 2004). For these reasons the  
219 calculation of riverine primary production, via aquatic photosynthesis, has been omitted in the  
220 model calculations.

221 In the river, the imported organic matter is decomposed by manual breakup by either abiotic  
222 decomposition like grinding or by biotic fragmentation by shredders such as Gammaridae, or fish  
223 (Hedges et al., 1994; Martius, 1997; Melack and Forsberg, 2001). Moreover, *decomposition*  
224 includes the leaching of coarse and fine material to form dissolved organic carbon (*DOC* in Fig.  
225 2) (Lampert and Sommer, 1999). This enlarges the surface for colonization by fungi and bacteria  
226 which are responsible for biochemical decomposition (*respiration*) (Martius, 1997; Wantzen et  
227 al., 2008). During heterotrophic respiration, most of the ingested carbon is released as  $\text{CO}_2$  to the  
228 water body (*IC* in Fig. 2).

229 *Outgassing*, i.e. evasion of gases from the water body, occurs, when the concentration of a  
230 specific gas in the water body exceeds its saturation concentration which depends on temperature  
231 and partial pressure (Schwoerbel and Brendelberger, 2005). Due to high carbon input into the  
232 Amazonian rivers, large amounts of  $\text{CO}_2$  and  $\text{CH}_4$  are produced and saturate the water (Mayorga  
233 et al., 2005; Richey et al., 2002). The outgassing of  $\text{CO}_2$  contributes more than 95% to the total  
234 outgassed carbon (Belger et al., 2011; Melack et al., 2004; Richey et al., 2002). We therefore  
235 considered only the outgassing of  $\text{CO}_2$  in the model ( $\text{CO}_2$  in Fig. 2).

236 An overview of model input, comprising static data (describing fixed site conditions), and  
237 dynamic data, like climate, atmospheric  $\text{CO}_2$  concentration, and terrigenous organic carbon, is  
238 given in Table 1. Physical constants are listed in Table 2. The following sections describe the  
239 input data, modelling approach of individual processes and the coupling to LPJmL.

240 **Input data and RivCM model initialization**

241 *River type* and *river order* (Fig. 3), as well as *river area* which represents about 25% of the  
242 potential floodable area (Langerwisch et al., 2013; Richey et al., 2002), prescribe the size and  
243 characteristics of the river stretch. The *river type* of each cell was defined by combining  
244 information published by Sioli (1957), Irion (1976), and Diegues (1994), and can be either white,  
245 black or clear water. The river colour depends on the amount of sediments and dissolved organic  
246 material in the water. It determines amongst others the pH and the temperature. For  
247 simplification, very small catchments (smaller than the simulated resolution) of deviating river  
248 types were neglected and the dominant river type was used. River order is represented by three  
249 classes and defined by total annual discharge (headwater:  $< 8 \times 10^3 \text{ m}^3 \text{ yr}^{-1}$ ; middle reach:  $8 \times 10^3$   
250 to  $2 \times 10^5 \text{ m}^3 \text{ yr}^{-1}$ ; lower reach:  $> 2 \times 10^5 \text{ m}^3 \text{ yr}^{-1}$ ). We chose these classes because of their  
251 different characteristics, as it is discussed in the River Continuum Concept (Vannote et al.,  
252 1980). Each grid cell that receives the routed water (*rout cell*) is determined by a digital  
253 elevation model (as also in Rost et al., 2008). The water is routed with a slope depending flow  
254 velocity  $v$  [ $\text{m s}^{-1}$ ] (Langerwisch et al., 2013), which results in a distance that is routed through  
255 per month of about 13 cells (in the largest part of the basin).

256 Data input from LPJmL to RivCM

257 Monthly discharge ( $Mdis$  [ $\text{m}^3 \text{ s}^{-1}$ ]), amount of water ( $Mwat$  [ $\text{m}^3$ ]), soil water content for two soil  
258 layers ( $Mswc_1$  within the upper soil layer ( $soildepth_1=200\text{cm}$ ) and  $Mswc_2$  within the lower soil  
259 layer ( $soildepth_2=300\text{cm}$ ) [%]) are provided by LPJmL. Additionally, annual litter carbon ( $ALitc$   
260 [ $\text{g m}^{-2}$ ]) and soil carbon ( $ASoilc$  [ $\text{g m}^{-2}$ ]) are provided by LPJmL (see also Figs. 1 and 2). The  
261 coupling is unidirectional. RivCM uses the LPJ output as input, but the processes calculated are  
262 only affecting the carbon pools and fluxes in RivCM. The carbon stored in litter and soil is  
263 calculated in LPJmL, while for simplification the reduction of litter due to the mobilization is not  
264 fed back to LPJmL.

265 Atmospheric  $\text{CO}_2$  concentration ( $atmCO_2$  [ppm]) and monthly temperature ( $T$  [ $^\circ\text{C}$ ]) prescribing  
266 abiotic atmospheric conditions are derived from the climate input data sets (see section 2.2).

267 Water temperature

268 Water temperature at time  $t$  [ $^\circ\text{C}$ ] depends on air temperature ( $T_{air_t}$ ) [ $^\circ\text{C}$ ] and river colour, given  
269 by *river type*. In white and clear water rivers the temperature is below air temperature. The  
270 calculation of water temperature of these rivers is conducted according to Eq. (1) based on  
271 Bogan et al. (2003), with  $T_t$  calculated as

$$T_t = 0.6946 \times T_{air_t} + 5.19 \quad (1)$$

272 The temperature in black water rivers is close to air temperature.



273 Temperature response

274 The respiration reaction calculated in RivCM at time  $t$  is adjusted according to the water  
 275 temperature  $T_t$  by a coefficient for temperature response  $Tresponse_t$  (Eq. (2) (Lampert and  
 276 Sommer, 1999). Additionally to the temperature response in water (and water saturated soil), a  
 277 temperature response for (unsaturated) soils was calculated with Eq. (3).

$$Tresponse_t = e^{308.56 \times (\frac{1}{56.02} - \frac{1}{T_t + 46.02})} \quad (2)$$

$$Tresponse_{dry_t} = Tresponse_t \times \frac{1 - (e^{-\frac{Mswc_1 \times soildepth_1 + Mswc_2 \times soildepth_2}{soildepth_1 + soildepth_2}})}{1 - (e^{-1})} \quad (3)$$

278 This is based on the empirical relationship of temperature response in soils (Lloyd and Taylor,  
 279 1994, also applied in LPJmL) which is valid for temperatures above  $-40^\circ\text{C}$ .

280 **Initialization of litter and soil carbon**

281 As initialization for  $Litc$  and  $Soilc$  in the first simulated month, RivCM uses the litter and soil  
 282 carbon stocks ( $ALitc$ ,  $ASoilc$ ) from LPJmL. Analogue to LPJmL, a further division of  $Soilc$  into a  
 283 fast respiring fraction (10%  $Soilc_{fast}$ ) and a slow respiring fraction (90%  $Soilc_{slow}$ ) was calculated.  
 284 Additionally, the annually produced litter prior respiration is used in RivCM. Since LPJmL does  
 285 not account for inundation, which changes respiration, the respiration of litter in (partly) water-  
 286 saturated soils is calculated within RivCM.

287 In general, in tropical forests litter falls continuously throughout the year (Müller-Hohenstein,  
 288 1981). In forests, where the flooding triggers litter fall, a peak of litter fall occurs during rising  
 289 and high water stage (Irmler, 1982). Because this is not accounted for in LPJmL (Sitch et al.,  
 290 2003), the annual un-respired litter carbon pool provided by LPJmL,  $ALitc_{unresp}$  was  
 291 heterogeneously partitioned over 12 months to initialize the monthly litter amount ( $Litc_{unresp}$ ) in  
 292 RivCM (Fig. 2, INPUT box). With Eq. (4) and Eq. (5) the maximum amount of carbon was  
 293 distributed to the month with high water and the minimum (at least 10% of annual litter) was  
 294 distributed to the month with low water. This depended on the distance between the current  
 295 month to the distance between the month with high water peak and the month with low water  
 296 peak ( $dist_{highlow}$ ). With this approach we achieved a skewed distribution of litter carbon. The  
 297 factor for the monthly fraction ( $fraction_{m_t}$ ) was calculated with

$$fraction_{m_t} = \cos\left(\frac{m_t}{dist_{highlow}} \times \pi\right) + (1.0 + litfrac_{min}) \quad (4)$$

298 if the current month number ( $m_t$ ; from 0-11) is smaller than the distance between high and low  
 299 water peak ( $dist_{highlow}$ ), to distribute the maximum amount of carbon to the month with high  
 300 water, or with

$$fraction_{m_t} = -\cos\left(\frac{m_t - dist_{highlow}}{12 - dist_{highlow}} \times \pi\right) + (1.0 + litfrac_{min}) \quad (5)$$

301 if the current month number ( $m_i$ ; from 0-11) is larger than the distance between high and low  
 302 water peak ( $dist_{highlow}$ ) to distribute the minimum amount of carbon ( $\geq 10\%$  of annual litter) to  
 303 the month with low water. Equation (4) calculates the convex part of the function, while Eq. (5)  
 304 calculates the concave part of the function. The first part of both equations represents the cosine  
 305 portion, and the second part sets the minimum of litter for the month with the low water peak  
 306  $litfrac_{min}$ .

307 By calculating the fraction of current monthly litter production versus total litter production in  
 308 the course of each year (Eq. (6)), the total monthly un-respired litter carbon ( $LitC_{unresp_t}$ ) can be  
 309 determined with Eq. (7).

$$mfraction_t = \frac{fraction_{m_t}}{\sum_{t=0}^{11} fraction_{m_t}} \quad (6)$$

$$LitC_{unresp_t} = mfraction_t \times ALitC_{unresp} \quad (7)$$

### 310 **Respiration of litter and soil carbon**

311 The initialized litter and soil carbon pools ( $LitC$ ,  $SoilC$ ) are respired and re-filled with the amount  
 312 of the respiration of un-respired litter carbon ( $LitC_{unresp}$ ). The calculation of respiration of organic  
 313 matter depends on soil water content and temperature. The soil water content ( $M_{swc}$ ) in un-  
 314 inundated grid cells was provided by LPJmL, while the soil water content of (partly) inundated  
 315 cells was calculated depending on the fraction of cell covered with water in RivCM. In inundated  
 316 parts of the grid cell the soil water content was set to 100%. The respiration of the un-respired  
 317 litter carbon and the soil carbon was calculated analogous to the LPJmL routine (for details see  
 318 also SI Eqs. (S1) to (S12)) and is updated in each time step.

### 319 **Mobilization**

320 The mobilization function calculates the amount of mobilized terrestrially fixed carbon  
 321 dependent on the amount of available exportable organic carbon on land, and on the size of  
 322 inundated area. This area is determined using current discharge, reference discharge and  
 323 potentially floodable area. The mobilization is not dependent on the river type, since the physical  
 324 conditions of moving water to mobilize terrigenous material are the same on black and white  
 325 water rivers.

#### 326 Size of monthly inundated area

327 The inundated area at time  $t$  ( $InunArea_t$  [km<sup>2</sup>]) was defined as the area covered by water,  
 328 including river and floodplain. It is determined by the current monthly discharge ( $Mdis_t$  [m<sup>3</sup> s<sup>-1</sup>])  
 329 relative to the mean maximum discharge of the reference period 1971-2000 ( $RefMeanMaxMdis$   
 330 [m<sup>3</sup> s<sup>-1</sup>]) produced under the climate forcing of CRU TS2.1 (Österle et al., 2003; Mitchell and  
 331 Jones, 2005). The potentially floodable inundated area ( $MaxInunArea$  [km<sup>2</sup>]) Langerwisch et al.,

332 2013) (Eq. (8)  $MaxInunArea$  [km<sup>2</sup>] was calculated using the fraction of the cell that is potentially  
 333 floodable (Langerwisch et al., 2013) multiplied by the cell area. The potentially floodable area  
 334 was calculated by applying a modified Topographic Relative Moisture Index (based on Parker,  
 335 1982) to a digital elevation model provided by the WWF database HydroSHEDS (WWF  
 336 HydroSHEDS, 2007) as described by Langerwisch et al. (2013).

$$InunArea_t = \frac{Mdis_t}{RefMeanMaxMdis} \times MaxInunArea \quad (8)$$

337 If the current monthly discharge is very high and thereby larger than the mean maximum  
 338 discharge of the reference period, the inundated area can exceed the potentially floodable area.

339 Because the export of terrigenous organic material is highest close to the river, each cell is  
 340 subdivided into six sections, to account for spatial differentiation depending on the vicinity to the  
 341 river. The size of the sections one to five is calculated with an exponential function (Eq. (9)). The  
 342 remaining cell area is allocated to section six. The river area is assigned to the cell sections  
 343 starting from the smallest section (Fig. S1). The river can expand into the next larger section  
 344 during rising water. The largest section has the largest distance to the river and is therefore only  
 345 occasionally inundated.

$$size_{section} = \frac{1}{e^{(number_{section}+1)}} \quad (9)$$

346

#### 347 Size of floodplain area

348 The floodplain area ( $FloodplainArea$  [km<sup>2</sup>]) at time  $t$  equals the inundated area that is not  
 349 permanently covered with water. It was calculated by subtracting the river area (25% of  
 350 inundated area, Richey et al., 2002) from the inundated area using Eq. (10) (see also  
 351 Langerwisch et al., 2013).

$$FloodplainArea_t = InunArea_t - (0.25 \times MaxInunArea) \quad (10)$$

#### 352 Amount of exported litter and soil carbon

353 This function calculates the amount of carbon exported from the terrestrial litter and soil pools to  
 354 the river. River and forests at the headwater, which is defined by an annual discharge of less than  
 355  $8 \times 10^3 \text{ m}^3 \text{ yr}^{-1}$  (river order 1 in Fig. 3B), are assumed to be much closer interconnected than at  
 356 middle and lower reaches (order 2 and 3). Since small streams at the headwater directly flow  
 357 beneath the trees, their export of litter and soil carbon was calculated from the entire inundated  
 358 area. In all cells of higher river orders the export of terrestrial organic material occurs in the  
 359 model only from the floodplain area and not from the permanently flooded river.

360 The *Igapó* forests which are inundated by black water rivers produce approximately 35% less  
 361 litter and soil carbon (Worbes, 1997) compared to white water inundated *Várzea* forests. LPJmL

362 simulates tropical rainforest which is analogue to *Várzea*. Since LPJmL does not account for the  
 363 different forest types, a correction of the organic material is performed for the *Igapó* forests.  
 364 Hence, the amount of exportable organic material from the black water cells at time  $t$  is reduced  
 365 by a factor of 0.35 ( $1 - carboncorr$ ; details in Table 3, Eqs. (11) and (12)).

$$Litc_{t_{corr}} = Litc_t \times carboncorr \quad (11)$$

$$Soilc_{t_{corr}} = Soilc_t \times carboncorr \quad (12)$$

366 For simplicity the following equations do only refer to  $Litc$ , instead of to the corrected value  
 367  $Litc_{corr}$  in case of *Igapó*.

368 The mobilization of litter and soil carbon at time  $t$  ( $mLitc_t$ ,  $mSoilc_t$ , [ $10^6$  g C cell $^{-1}$ ]) is calculated  
 369 using the specific mobilization rates for litter and soil carbon (Table 3, Eqs. (13) and (14)).

$$mLitc_t = Litc_t \times FloodplainArea_t \times mobil_{litter} \quad (13)$$

$$mSoilc_t = Soilc_t \times FloodplainArea_t \times mobil_{soilc} \quad (14)$$

370 According to Irmeler (1982), litter carbon is mobilized with a rate of 0.4 month $^{-1}$ . After a  
 371 sensitivity analysis this rate ( $mobil_{litter}$ ) was calibrated to 0.7 month $^{-1}$  (see SI). Soil carbon  
 372 mobilization takes place at a much smaller rate. Since no detailed value is available, the rate of  
 373 soil mobilization ( $mobil_{soilc}$ ) was calibrated after a sensitivity analysis to 0.05 month $^{-1}$ . Mobilized  
 374 carbon [ $10^6$  g C cell $^{-1}$ ], originating from litter and soil, consists of a particulate ( $mPOC_t$ ) and a  
 375 dissolved ( $mDOC_t$ ) carbon pool with the fractions of  $mobil_p$  and  $(1.0 - mobil_p)$ , respectively  
 376 (Table 3, Eqs. (15) and (16)).

$$mPOC_t = (mLitc_t + mSoilc_t) \times mobil_p \quad (15)$$

$$mDOC_t = (mLitc_t + mSoilc_t) \times (1.0 - mobil_p) \quad (16)$$

377 The fraction of mobilized particulate carbon ( $mobil_p$ ) was set to 0.5 according to McClain and  
 378 Elsenbeer (2001) and Johnson et al. (2006) and was evaluated in a sensitivity analysis (SI).

### 379 **Decomposition**

380 Depending on the rate of decomposition ( $decomp$  [month $^{-1}$ ], Table 3), the model calculates the  
 381 conversion from particulate ( $mPOC_t$ ) into dissolved organic carbon ( $dDOC_{t+1}$ ) which has been  
 382 estimated to be about 0.3 month $^{-1}$  by Furch and Junk (1997). In the calculations this rate was  
 383 modified according to the river type. Along black water rivers the leaves are more sclerophyllous  
 384 and thus much slower degradable (Furch and Junk, 1997). Therefore, the decomposition rate in  
 385 black water cells is reduced by factor 0.9 ( $1.0 - decompcorr$ ) based on Furch and Junk (1997)

386 (Table 3). The decomposed particulate organic carbon at time  $t$   $dPOC_t$  (Eq. (17)) was removed  
 387 from the particulate organic carbon pool and added to the dissolved organic carbon pool  
 388 (Eqs.(18) and (19)). The dissolved organic carbon is not fragmented any further.

$$dPOC_t = mPOC_t \times decomp \times decompcorr \quad (17)$$

$$dPOC_{t+1} = mPOC_t - dPOC_t \quad (18)$$

$$dDOC_{t+1} = mDOC_t + dPOC_t \quad (19)$$

### 389 Respiration

390 The respiration function calculates the decrease of particulate and dissolved organic carbon  
 391 ( $dPOC_{t+1}$ ,  $dDOC_{t+1}$ , [ $10^6$  g C cell<sup>-1</sup>]) by the respiration loss ( $rPOC_{loss}$  and  $rDOC_{loss}$ ) and the  
 392 associated increase of dissolved inorganic carbon ( $rIC_{t+1}$ ) at time  $t$  (Eqs. (20) to (24)). For this, a  
 393 sufficient abundance of respiring organisms is assumed. In contrast to different decomposition  
 394 rates in black and white water rivers, which is due to the fact that leaves at black water rivers  
 395 tend to be more sclerophyllous and therefore less easily degradable, for the respiration of already  
 396 degraded organic material we assume only minor differences. As soon as the leaves and twigs  
 397 are degraded to small particles we assume that they react similarly. Therefore, respiration only  
 398 depends on the rate of respiration loss ( $respi$  [month<sup>-1</sup>], see Table 3) and the temperature  
 399 response ( $Tresponse$ , Eq. (2)).

$$rPOC_{loss} = dPOC_{t+1} \times (1 - e^{-(respi \times Tresponse_t)}) \quad (20)$$

$$rDOC_{loss} = dDOC_{t+1} \times (1 - e^{-(respi \times Tresponse_t)}) \quad (21)$$

$$rPOC_{t+1} = dPOC_{t+1} - rPOC_{loss} \quad (22)$$

$$rDOC_{t+1} = dDOC_{t+1} - rDOC_{loss} \quad (23)$$

$$rIC_{t+1} = IC_t + rPOC_{loss} + rDOC_{loss} \quad (24)$$

### 400 Outgassing

401 The model calculates the monthly saturation concentration of CO<sub>2</sub>  $saturationC_t$  in the water  
 402  $Mwat_t$  [m<sup>3</sup>] (Eq. (25))

$$saturationC_t = k_H^\theta \times e^{d \ln k_H \times \left( \frac{1}{T_t + 273.15} - \frac{1}{T^\theta} \right)} \times \frac{atmCO_{2t}}{10^6} \times ctoco2 \times Mwat_t \times 10^3 \quad (25)$$

403 using Henry's Law (Sander, 1999) and applying Henry's law constant ( $k_H^\theta$  [g CO<sub>2</sub> l<sup>-1</sup> atm<sup>-1</sup>])  
 404 under standard conditions ( $T^\theta = 298.15\text{K}$ ), temperature dependence of the Henry's law constant  
 405 ( $d\ln k_H$  [K]), the ratio of carbon to carbon dioxide ( $ctoco2$ ), and monthly temperature  $T_t$  in °C.  
 406 Depending on the river type, which determines the pH of the water, we calculated the amount of  
 407 CO<sub>2</sub>, HCO<sup>3-</sup> and CO<sub>3</sub><sup>2-</sup>. For calculating the actual outgassing we only take the carbon into  
 408 account, instead of the chemical form in which it exists. Afterwards, monthly saturation is  
 409 multiplied with a monthly saturation factor ( $co2satur$ , Eq. (26), Table 3), which accounts for the  
 410 super-saturation of the water with CO<sub>2</sub>. These values depend on the hydrograph and were  
 411 extracted from Richey et al. (2002). The difference between inorganic carbon amount and  
 412 saturation concentration was added to the atmosphere carbon pool ( $ICoutgas_{t+1}$ , Eq. (27)), while  
 413 carbon in the river equals the saturation concentration ( $oIC_{t+1}$ , Eq. (28)).

$$saturationCcorr_t = saturationC_t \times co2satur \quad (26)$$

$$ICoutgas_{t+1} = ICoutgas_t + (rIC_{t+1} - saturationCcorr_t) \quad (27)$$

$$oIC_{t+1} = saturationCcorr_t \quad (28)$$

## 414 2.2 Climate data sets

415 For model evaluation, climate forcing data from a homogenized and extended CRU TS2.1 global  
 416 climate dataset (Österle et al., 2003; Mitchell and Jones, 2005) were used. Annual atmospheric  
 417 CO<sub>2</sub> concentrations were prescribed as given by Keeling and Whorf (2003).

418 For the assessment of climate change impacts, three SRES scenarios (A1B, A2, B1)  
 419 (Nakićenović et al., 2000) were applied. Five General Circulation Models (GCMs) (Jupp et al.,  
 420 2010; see also Randall et al., 2007), namely, MIUB\_ECHO\_G, MPI\_ECHAM5, MRI\_CGCM2\_3\_2A,  
 421 NCAR\_CCSM3\_0, UKMO\_HADCM3 were chosen to cover a wide range of uncertainty within  
 422 climatic projections with respect to precipitation patterns and temperature. The GCMs used the  
 423 SRES scenarios to calculate future climate. For example, the model MIUB\_ECHO\_G shows a  
 424 shortening of the dry season (defined by less than 100 mm precipitation per month), whereas  
 425 UKMO\_HADCM3 shows an elongation of the dry season towards the end of the century.  
 426 Temperature in the Amazon basin is projected to increase under the A1B emission scenario by  
 427 about 3.5K, by up to 4.5K for A2, and by up to 2 to 2.5K for B1 until the end of the century  
 428 (Meehl et al., 2007). Projected rainfall differs considerably in spatial distribution within the  
 429 Amazon basin among climate models. Under A1B, for instance, a decrease in precipitation is  
 430 projected for Southern Amazonia (especially during the southern-hemisphere winter), whereas  
 431 an increase in precipitation is projected in the Northern part (for details see Meehl et al., 2007).  
 432 The projected climate data were bias-corrected with the CRU TS2.1 global climate dataset

433 (Österle et al., 2003; Mitchell and Jones, 2005). Annual future atmospheric CO<sub>2</sub> concentrations  
434 are based on the respective SRES scenario.

435 All monthly climate data (observed and projected) were disaggregated to 'quasi-daily' values as  
436 described by Gerten et al. (2004).

### 437 **2.3 RivCM calibration and evaluation**

438 To identify the most important explaining variables (parameters) and the most sensitive response  
439 variables (carbon pools), a redundancy analysis (RDA) was performed. Based on the analysis we  
440 calibrated *mobil<sub>litc</sub>* and *mobil<sub>soilc</sub>* (see SI).

441 To evaluate the performance of RivCM, a comparison of observed with simulated data was  
442 conducted. TOC, POC, and DOC concentration were chosen, as well as exported carbon to the  
443 ocean (TOC, POC, and DOC per year) and exported carbon to the atmosphere (outgassed CO<sub>2</sub>  
444 per year on different spatial domains) (see Table 4). The estimates of carbon exported to the  
445 Atlantic Ocean are from the gauging station at Óbidos. The data from this station represent an  
446 integration of information over the entire Amazon basin. Therefore they do not reflect large  
447 temporal or spatial deviation over the basin and enable us to compare aggregated measured data  
448 with aggregated simulated data. If possible, data from the same time period were compared. If  
449 the observation period was after the last simulation year 2003, the data were compared to  
450 simulated values from the reference period (1971-2000). The results of the evaluation can be  
451 found in the SI.

### 452 **2.4 Modelling protocol and simulation experiments**

453 We performed LPJmL simulations with potential natural vegetation only, i.e. without land use,  
454 on a 0.5° × 0.5° spatial resolution. To obtain equilibria for vegetation distribution, carbon and  
455 water pools in LPJmL, all transient LPJmL runs were preceded by a 1000-years-spinup during  
456 which the pre-industrial CO<sub>2</sub> level of 280 ppm and the climate of the years 1901-1930 were  
457 repeated. All transient runs of the coupled model LPJmL-RivCM were preceded by a 90-years-  
458 spinup during which the climate and CO<sub>2</sub> levels of 1901-1930 were repeated to obtain equilibria  
459 for riverine carbon pools. Transient climate simulations are then performed for current climate  
460 (1901-2003) and future climate (2004-2099). The data sets used are described in the section 2.2.

461 To identify how relevant the amount of riverine outgassed carbon for the basin-wide carbon  
462 budget in a changing climate is, we compared the output of coupled-terrestrial-riverine  
463 modelling runs with purely terrestrial or purely riverine modelling settings. The three different  
464 factorial settings are the following:

465 Setting 1 (*Standard*) refers to the standard RivCM simulation including the actual river and the  
466 additionally inundated area. In these simulations the export of organic material from the land

467 to the river was calculated, as well as the discharge of carbon to the ocean, aquatic outgassing  
468 and release of CO<sub>2</sub> via terrestrial heterotrophic respiration.

469 Setting 2 (*NoInun*) includes the actual river, but excludes additional inundation. For this purpose,  
470 the cell fraction, which is not permanently covered by water, remains dry to emulate no  
471 coupling of land and river. In this simulation experiment no export of organic material from  
472 the land to the river was calculated (i.e. there is no input of terrigenous organic material into  
473 the river). Hence, no discharge of carbon to the ocean, no outgassing, but release of CO<sub>2</sub> from  
474 the terrestrial heterotrophic respiration was calculated.

475 Setting 3 (*NoRiv*) includes calculations in which the original LPJmL results for CO<sub>2</sub> release from  
476 vegetation only were used, i.e. the influence of the river and inundation were not accounted  
477 for. In these simulations no outgassing from the water and no discharge of carbon to the ocean  
478 was calculated. In contrast, outgassing from the heterotrophic respiration of the forest, also in  
479 the areas in which RivCM simulates river area, was calculated.

480 In a full factorial design, all inundation scenarios (*Standard*, *NoInun* and *NoRiv*) were run for all  
481 climate scenarios for future and current climate.

## 482 **2.5 Analyses of future changes in the coupled terrigenous-riverine system**

483 The effect of climate change is estimated by calculating the differences between carbon values in  
484 a future period (2070-2099) and a reference period (1971-2000). Four different carbon pools  
485 were analysed, namely outgassed carbon (atmospheric), riverine particulate organic carbon  
486 (POC) and dissolved organic carbon (DOC), as well as the riverine inorganic carbon pool (IC)  
487 and. The relative changes in POC and DOC are spatially and temporally similar (Fig. S4).  
488 Therefore, only POC is shown and discussed in detail.

489 The spatial distribution of climate change effects ( $E_{CC}$ ) on the different carbon pools and fluxes  
490 (indicated by  $_n$ ) were estimated by calculating for each cell the quotient (Eq. (29)) of future values  
491 (mean of 2070-2099) and reference values (mean of 1971-2000). To equalize a tenfold increase  
492 ( $10^{+1}$ ) and a reduction to one tenth ( $10^{-1}$ ), the quotient was log-transformed ( $\log_{10}$ ).

$$E_{CC_n} = \log_{10} \frac{\sum_{n=2070}^{2099} C_n}{\sum_{n=1971}^{2000} C_n} \quad (29)$$

493 To show model uncertainty that arises from differences in climate model projections an indicator  
494 of the agreement between simulation results was calculated, it indicates a common significant  
495 increase or decrease, respectively, of three, four or all five climate models. In addition, the  
496 significance (p-value <0.05) of the difference between reference and future was assessed by a  
497 Wilcoxon Rank-Sum Test (Bauer, 1972). This test can be used for datasets that are not normally  
498 distributed and is therefore applicable to these data with high intra-annual fluctuations.



499 Additionally to the analysis of spatial patterns, an analysis of changes in mean carbon pools over  
500 time was conducted. As above, changes were expressed as the logarithm of the quotient between  
501 annual future values and mean reference values. In addition to these relative changes, the  
502 absolute values in both periods were compared. The analysis was conducted both for the whole  
503 Amazon basin and for three selected subregions. These three regions, indicated in Fig. 6A, were  
504 identified according to future changes in inundation patterns, discussed in Langerwisch et al.  
505 (2013). These areas include a region in the Western basin with projected increase in inundation  
506 length and inundated area (R1), a region covering the Amazon main stem (R2) with intermediate  
507 changes in inundation and a region with projected decrease in duration of inundation and  
508 inundated area (R3). For details of the exact position of these regions see Table 5.

509 All statistical analyses were conducted using several packages in R. For the sensitivity analysis  
510 the package 'vegan' (Oksanen et al., 2011) and for the analysis of the projections the packages  
511 'stats' (R Development Core Team and contributors worldwide, 2011) and 'maptools' (Lewin-  
512 Koh and Bivand, 2011) were used.

513

## 514 **3 Results**

515

### 516 **3.1 Validation of the simulation results**

517 To assess the potential changes of the riverine carbon pools and fluxes, it is essential that we  
518 trust the model's ability reproduce observed patterns and fluxes. For this, the first step is to  
519 validate river discharge before assessing carbon pools and fluxes. This has been done in  
520 Langerwisch et al. (2013) for 44 gauging stations in the Amazon basin, and shows that the  
521 observed discharge patterns can be reproduced. Here, we validated the carbon concentration and  
522 export fluxes with published data (Table 4). If possible we compared the simulated with  
523 observed values from the same period of time. We only included spatial data for which we could  
524 find the exact location (longitude/latitude).

525 The validation of exported data shows that the outgassed carbon (export to the atmosphere) is  
526 underestimated by the model on a small scale by more than 90% and on the basin wide scale by  
527 70%. In contrast the organic carbon exported to the ocean is overestimated by the model by 70%.  
528 However, on a sub-catchment level the overestimation of exported organic carbon is much  
529 smaller. Comparing observed and simulated concentrations of POC, DOC and IC shows that  
530 simulation results are within the observed range. For POC the simulated concentration is about  
531 50% larger than the observed concentration, but with a range between -90% and +200%. For the

532 simulated DOC concentration the range is between -90% and +90%, while for IC the range is  
533 between -70% and +60%.

534

### 535 **3.2 Changes in riverine carbon under future climate projections**

536 The amount of outgassed carbon (Fig 4A) is simulated to remain constant compared to 1971-  
537 2000 until about 2020. This is followed by a clear increase. This increase is strongest in in region  
538 R1 (mean +70%) while it is moderate in R2 and R3 (+30% and +20%, respectively). Generally,  
539 the simulated increase is largest for the SRES A2 scenario, followed by the A1B and the B1  
540 scenario (see also Fig. 5). The spread of simulated outgassed carbon is comparably large between  
541 the five climate models. Outgassed carbon shows a basin wide increase (Fig. 6G-I). In most parts  
542 of the basin the outgassed carbon increases only slightly but significantly ( $p < 0.05$ ; up to 2-fold).  
543 In parts of the Andes the increase is up to 5-fold, shown by at least four of the five climate  
544 models (as indicated by crosses in Fig. 6). In a few areas in the Southern Andes the outgassed  
545 carbon decreases (0.3-fold).

546 The changes in POC (Fig. 4B) show a slight basin wide increase of about +10% (SRES mean)  
547 until the end of the century. In region R1 this increase is larger, with +50% (SRES A2) and  
548 +35% (SRES B1). In the regions R2 and R3 the POC amounts remain nearly constant (+5% and  
549  $\pm 0\%$ , respectively). A wide range of possible paths of simulated POC amounts is spanned by the  
550 five climate models, whereas the three emission scenarios only result in minor differences in  
551 simulation results (see also Fig. 5). The spatial changes for POC show an up to 2-fold increase in  
552 the Western and South-Western part of Amazonia for all three SRES emissions scenarios (Fig.  
553 6A-C) with high agreement between the five climate models compared to the reference period.  
554 In contrast, climate model agreement in the Northern and North-Western basin is lower and  
555 shows a decreasing trend in the POC pool with a factor of 0.5. For the central part of the basin,  
556 no clear trend is visible. POC seems to be less sensitive to different changes in atmospheric  $\text{CO}_2$   
557 concentrations compared to IC as only small regional differences were simulated with POC  
558 increasing in the Western part of the basin under the A2 scenarios and decreasing in the Northern  
559 part of the basin under the A1B scenario.

560 In contrast to outgassed carbon and DOC, riverine inorganic carbon (IC) increases basin wide  
561 (Figs. 4C and 5) during the entire 21<sup>st</sup> century. Here, clear differences in the SRES emission  
562 scenarios are found. In the SRES A2 scenario the increase is largest, with a basin wide increase  
563 by +150% (+220% in R1, +150% in R2, and +140% in R3). In the B1 scenario the average  
564 increase is smallest, with basin wide +50% (+80% in R1, +60% in R2, and +50% in R3). The  
565 spatial distribution of changes in riverine inorganic carbon (IC, Fig. 6D-F) shows an overall  
566 increase compared to the reference period. For at least four climate models this increase in IC is  
567 significant ( $p < 0.05$ ), especially in the Western part of the basin. Here, the largest changes are  
568 found for the SRES emission scenario A2 (up to 5-fold increase).

569 **3.3 Changes in the export of riverine carbon to ocean and atmosphere under**  
570 **future climate**

571 Riverine outgassed carbon makes up on average 10% of total outgassed carbon along the river  
572 network during the reference period (Fig. 8A). Total outgassed carbon includes carbon evaded  
573 from the river and the forest. The carbon evaded from the forest reflects the amount of terrestrial  
574 respired carbon (autotrophic and heterotrophic respiration). The average changes in this  
575 proportion caused by climate change and the agreement of climate models (indicated by crosses)  
576 on the direction of change are depicted in the three maps in Fig. 8B-D. The largest differences  
577 are found under the SRES A2 scenario with the largest area in agreement between the climate  
578 models (Fig. 8C). Here an increase of up to 7% in the proportion is found in the Western and  
579 South-Western part of the Amazon basin. This increase is less pronounced in the other two  
580 emission scenarios (Figs. 8B and 8D). For all SRES scenarios a slight decrease in the proportion  
581 of up to 2% (-0.02) can be seen in parts of the North-Western basin and scattered in the very  
582 South (Fig. 8B-D), this occurs because rivers will contribute increasingly to respiration losses of  
583 carbon.

584 To estimate the relevance of riverine carbon to imported atmospheric carbon (via terrestrial  
585 photosynthesis) or exported carbon (via outgassing or discharge to the ocean), results of the  
586 factorial experiments were compared (Wilcoxon Rank-Sum Test;  $p < 0.001$ , Table 6, see also  
587 section 2.4). The standard RivCM results (*Standard*) were analysed to estimate the role of  
588 riverine carbon to total carbon export. The simulated mean annual total organic carbon (TOC)  
589 discharged to the ocean during the reference period (1971-2000) is about  $54 \times 10^{12} \text{ g yr}^{-1}$  (Table  
590 6). This represents approximately 1.0% of the basin net primary production (NPP). The export of  
591 TOC to the ocean changes under climate change depends on the three SRES emission scenarios.  
592 In the A1B scenario mean annual export decreases significantly by about 8.9% for 2070-2099  
593 (compared to the reference period) for all five climate models, whereas under the A2 scenario the  
594 TOC export increases by about +9.1%. The B1 scenario shows an intermediate change, with an  
595 increase of about +4.6%. Depending on the emission scenario, the export of TOC to the ocean  
596 decreases from about 1% of the NPP to about 0.75-0.9% of the NPP in the future period.

597 **3.4 Summary of overall changes in the carbon fluxes under climate change**

598 The first three research questions we addressed in this study were answered with the above  
599 mentioned results. As a summary Fig 7 provides an aggregated picture of projected changes in  
600 terrestrial carbon pools and resulting changes in riverine carbon pools. The moderate increase in  
601 terrestrial carbon (on average +12.7% in biomass, +13.8% in litter carbon and +4.1% in soil  
602 carbon) leads to a moderate increase of riverine organic carbon (POC +10.7% and DOC +8.3%),  
603 but due to an increased  $\text{CO}_2$  partial pressure the outgassed carbon increases by about 42.6%,  
604 whereas the discharged carbon increases only by about 1.1%.

605

### 606 **3.5 Relevance of the riverine outgassed carbon**

607 To assess the relevance of riverine carbon for total carbon export to the atmosphere, either from  
608 the forest (heterotrophic respiration) or from the water, the standard RivCM results (*Standard*)  
609 were compared to results of the *NoInun* experiment and the *NoRiv* experiment (Table 6). In the  
610 reference period the total outgassed carbon is estimated to be about  $440 \times 10^{12} \text{ g month}^{-1}$ ,  
611 calculated in the standard RivCM simulations (*Standard*). Under climate change this amount  
612 increases by 23%, 28%, and 21% for emission scenarios A1B, A2 and B1, respectively. The  
613 proportion of outgassed carbon from the river to total outgassed carbon is about 3.6% in the  
614 reference period. This proportion increases in all emission scenarios to up to 3.9% to 4.3%.  
615 During the reference period the amount of riverine outgassed carbon makes up about 3.5% of the  
616 net primary production (NPP). In the future this proportion increases significantly to up to  
617 4.25%.

618 The simulations without input of terrigenous organic material to the river, caused by suppressed  
619 inundation (*NoInun*), lead to a reduction of total outgassed carbon. During the reference period it  
620 is significantly reduced by about  $-3.30\%$ . During the future period this reduction remains  
621 relatively constant for all SRES scenarios. If the river area is substituted by potential forest cover  
622 (*NoRiv*), the total terrestrial outgassed carbon is about 0.1% lower than the sum of terrestrial and  
623 riverine outgassed carbon in the standard simulations. This proportion decreases slightly to 0.07-  
624 0.10% in the future period.

625

## 626 **4 Discussion**

627 The main goal of our study was to develop a coupled terrestrial-riverine model for assessing  
628 regional and global carbon budget, considering riverine carbon pools and fluxes and their  
629 potential changes under climate change. We used the Amazon basin as a case study because it  
630 represents a tightly coupled terrestrial-riverine system. To achieve our goal we combined the  
631 newly developed riverine carbon model RivCM with the terrestrial vegetation model LPJmL. In  
632 the following we discuss the performance of and uncertainties in the coupled model system, as  
633 well as the mechanisms leading to projected changes in riverine carbon. Finally, we elaborate on  
634 the importance of incorporating the terrestrial-riverine coupling in models to better understand  
635 processes in terrestrial-riverine systems.

#### 636 4.1 Riverine carbon pools

637 The model RivCM calculates the dynamics of several organic carbon pools and fluxes in the  
638 Amazon basin. A comparison of these carbon pools and fluxes with observation shows in  
639 summary that model results are within the range of observed concentrations of both organic and  
640 inorganic carbon pools, but the model strongly underestimates the outgassed carbon while it  
641 overestimates the carbon discharged to the ocean.

642 For the concentration of carbon the range of observations is large, mainly caused by the different  
643 characteristics of the sub-catchments. The concentration of organic and inorganic carbon is  
644 overestimated by the model for some sub-catchments, while it is underestimated for others. The  
645 sub-catchments differ in their specific characteristics, such as water, soil and vegetation. Amon  
646 and Benner (1996) for instance illustrated the large difference in the mineralization of organic  
647 carbon in clear, white and black waters. The model has difficulties to capture these differences.  
648 Thus, including more site specific information for the water, the vegetation and the  
649 characteristics of the river stretch could lead to a better match between observation and  
650 simulation. However, the standard deviation of the observation is large and for most of the cases  
651 the simulated concentration lies within the observed range. The mismatch between the  
652 observation and the simulation might also be caused by an over or underestimation of carbon  
653 exported to the river, which depends on the inundated area. The model takes the nonlinear  
654 change in inundated area during flooding only simplified into account, which might lead to an  
655 underestimation of flooded area. The relatively coarse spatial resolution might also be a reason  
656 for the underestimation of the flooded area. The fixed ratio of 25% of the potentially floodable  
657 area, representing the river, might be less applicable to areas in the headwater. We compared the  
658 fixed ratio of 25% against observation in the lowlands (e.g. Lauerwald et al., 2015; Lehner and  
659 Döll, 2004; Richey et al., 1990) and think that this ratio is reasonable for the Amazon lowland.  
660 However, misestimating the actual floodplain river might also lead to poor estimates of exported  
661 organic carbon. An additional cause of differences between observed and simulated (inorganic)  
662 carbon amount might be that the model does not take weathering, other carbon sources than  
663 terrigenous carbon, or the longer residence time of water in the flooded forests into account. In  
664 summary the main reasons for the mismatch between observations and simulations is due to  
665 some simplifications (spatially and within the processes) we applied.

666 For the comparison of exported carbon to either the ocean or the atmosphere the model tends to  
667 overestimate the discharge to the ocean, while it underestimates the outgassing. The amount of  
668 discharged carbon is tightly coupled to the concentration and the water discharge. While the  
669 discharge of water has been shown to be realistic (Langerwisch et al., 2013), and the simulated  
670 concentration is within the observed range, a slight shift in the hydrograph can lead to the  
671 mismatch between observed and simulated amount of exported carbon to the ocean. In addition,  
672 the model might overestimate carbon exported to the ocean because it does not include dams.  
673 These artificial structures can lead to a prolonged residence time of water and its transported

674 material, and thus to prolonged decomposition and an increased sedimentation (Goulding et al.,  
675 2003). In the natural parts, such as floodplains, sedimentation especially impacts on the river bed  
676 structure (Allison et al., 1995; Junk and Piedade, 1997). However, the sedimentation of organic  
677 material is comparably small with only  $50 \text{ g C yr}^{-1}$  per square meter of water area (Melack et al.,  
678 2009). Sedimentation and resuspension act on the small to medium scale (Junk and Piedade,  
679 1997; Yarnell et al., 2006). On the spatial resolution of 0.5 degree both processes are assumed to  
680 be balanced for organic carbon and have therefore not been explicitly calculated in the model,  
681 but might be of importance at smaller scales. The amount of outgassed carbon from the water  
682 body of the river to the atmosphere is probably underestimated because the way RivCM  
683 calculates the inundated area and therewith the area of evasion does not include the cross-section  
684 of the riverbed. Therewith the non-linear increase of inundated area with an increase in water  
685 amount is not included. Including this would potentially lead to a larger inundated area, which  
686 would increase the outgassing. The temporal resolution of monthly time steps might also be a  
687 reason for the underestimation of the outgassing. In contrast to decomposition and respiration,  
688 which are calculated with fixed rates, the outgassing is variable and depends on the prescribed  
689 partial pressure of  $\text{CO}_2$  in the atmosphere and its calculated concentration in the water. Instead of  
690 using monthly time steps, an adjustment to a higher temporal resolution, leading to a more  
691 frequent exchange with the atmosphere, could potentially increase the amount of outgassed  
692 carbon.

693 For assessing the effects of climate change on riverine carbon and exported carbon pools and  
694 fluxes, we calculated their relative differences. Although the absolute simulated amounts and  
695 concentrations might not completely fit the observations, we are sure that the relative changes  
696 still provide insights into potential future changes.

697 The riverine carbon pools and fluxes in this tightly coupled system may change during the 21<sup>st</sup>  
698 century in several ways. According to our results climate change will induce a basin wide  
699 increase in riverine carbon pools. Areas most affected are the central and western basin. Here the  
700 outgassing of  $\text{CO}_2$ , as well as the organic and inorganic carbon pools increases most clearly.

701 Our results indicate that projected climate change may alter outgassed carbon ( $\text{CO}_2$  evasion) by  
702 several means. Firstly, a higher production of terrestrial material leads to an increase of organic  
703 carbon available for respiration; secondly, the higher atmospheric  $\text{CO}_2$  concentration leads to an  
704 increase in dissolved inorganic carbon in the water. Thirdly, higher water temperatures decrease  
705 the solubility of  $\text{CO}_2$  in the water, but also increase the respiration rates. Overall a combination  
706 of these factors may lead to a considerable increase in  $\text{CO}_2$  evasion and a slight increase of  
707 exported riverine carbon. Spatially the results are heterogeneous. The amount of outgassed  
708 carbon increases in most parts of the basin. This pattern is mainly driven by the increased  
709 amount of organic carbon available for respiration. However, even in areas where organic carbon  
710 does not increase, or even decreases, the amount of outgassed carbon is elevated. This is mainly  
711 caused by the increased respiration rate at higher temperatures. Thus, even with less carbon

712 available, higher temperatures lead to an elevated outgassing of CO<sub>2</sub>. As a consequence of an  
713 increased evasion of CO<sub>2</sub>, an additional increase in atmospheric CO<sub>2</sub> concentration can occur.  
714 However, the simulated amount of outgassed carbon under current conditions is underestimated  
715 in comparison to observations by a factor of up to 1/6. The observations are based on a  
716 combination of small scale measurements of CO<sub>2</sub> evasion and remotely sensed estimates of  
717 inundated area (Belger et al., 2011; Moreira-Turcq et al., 2003; Richey et al., 1990, 2002). In  
718 contrast, the outgassing calculated in RivCM is a more aggregated estimate. In reality during  
719 rising water stage, small changes in discharge can lead to a comparably larger non-linear  
720 increase in inundated area. This is not taken into account in RivCM. In RivCM the outgassing  
721 depends only on the inorganic carbon concentration in the water and the partial pressure of CO<sub>2</sub>.  
722 Additionally to the inundated area, also the vegetation coverage affects the outgassing of CO<sub>2</sub>  
723 from flooded area as Abril et al. (2014) show. Including the production of allochthonous organic  
724 material, which is not included in RivCM, might also change the amount of outgassed carbon.  
725 But in contrast to the other processes the production via photosynthesis might lead to an increase  
726 of the CO<sub>2</sub> evaded to the atmosphere. Furthermore, including the evasion of CO<sub>2</sub> from inundated  
727 soils, which represents a process that might lead to a further increase of simulated CO<sub>2</sub>  
728 outgassing, into RivCM would help to simulate outgassing that is more in agreement with  
729 observed estimates.

730 Besides riverine carbon fluxes such as outgassed carbon, climate change also affects riverine  
731 carbon pools. However, these changes are not homogeneously distributed across the basin. The  
732 increase in organic carbon (POC and DOC) is on one hand caused by the change in inundation  
733 patterns. This can be seen mainly in the Western part of the basin, resulting from an projected  
734 increase in precipitation, particularly in the SRES-A2 scenario (Langerwisch et al., 2013). On the  
735 other hand, more rainfall and increased atmospheric CO<sub>2</sub> concentration may lead to increased  
736 amounts of available organic carbon, i.e. more biomass under future climate conditions (e.g.  
737 Huntingford et al., 2013), which may directly increase the POC and DOC pools. As a  
738 consequence of the additional riverine organic carbon, a depletion of oxygen caused by enhanced  
739 respiration in the water can occur (Junk and Wantzen, 2004; Melack and Fisher, 1983). The  
740 resulting anoxia can lead e.g. to denitrification or production of methane (Lampert and Sommer,  
741 1999). In areas with already reduced O<sub>2</sub> levels, such as flooded forests during falling water, the  
742 further depletion of oxygen can potentially affect fish and other animal groups inhabiting the  
743 water (Hamilton et al., 1997; Melack and Fisher, 1983). The comparison with measured data  
744 (Cole and Caraco, 2001; Ertel et al., 1986; Hedges et al., 1994; Moreira-Turcq et al., 2003; Neu  
745 et al., 2011) shows that the concentrations of the different simulated carbon pools fit in the range  
746 of observations, with only a slight overestimation for POC. These results also show that the  
747 inclusion of allochthonous organic material is not necessarily needed to reproduce the observed  
748 POC concentrations in the water. The agreement of simulated with observed POC, DOC and IC  
749 concentrations shows the reliability of RivCM, because the errors in concentration measurements  
750 are small.

751 The amount of riverine inorganic carbon which remains in the water and does not evade to the  
752 atmosphere is projected to increase under climate change. Here, the lower solubility resulting  
753 from higher temperatures is not able to balance the effect of a higher atmospheric CO<sub>2</sub>  
754 concentration resulting in more dissolved CO<sub>2</sub>. This pattern is consistent within the emission  
755 scenarios and the climate models and can be found in most parts of the basin. The two- to  
756 threefold increase in inorganic carbon in the water might have serious consequences for fish and  
757 fungi, since dissolved inorganic carbon directly lowers the pH in the water (Lampert and  
758 Sommer, 1999). In combination with the oxygen depletion discussed above this might severely  
759 affect riverine fauna.

## 760 **4.2 Riverine outgassing and export to the Atlantic Ocean**

761 Our results indicate that climate change alters the proportion of carbon evaded from the river to  
762 carbon exported to the ocean. Climate change increases the outgassing of CO<sub>2</sub> with a higher rate  
763 than it increases the discharge of organic carbon.

764 During the reference period, the outgassed carbon from water bodies contributes on average  
765 about 3.6% of all evaded carbon from the entire Amazon basin. This seems to be only a small  
766 amount, but in river-dominated regions, this fraction may represent up to 10-50% of total evaded  
767 carbon, which is especially obvious in the Eastern part of the basin. The basin-wide proportion of  
768 riverine vs. total carbon evasion (including riverine outgassing and CO<sub>2</sub> release during  
769 autotrophic and heterotrophic respiration) increases from 3.6% to up to 4.3% from the reference  
770 to the future period, which indicates the increasing contribution of riverine outgassed carbon to  
771 the total outgassed carbon. Our results show that 3.5% of the carbon accumulated in terrestrial  
772 NPP is released to the atmosphere by outgassing from the river. It can be expected that climate  
773 change will alter this fraction to up to 4.2% which is caused by a combination of increased NPP  
774 and increased CO<sub>2</sub> partial pressure. Inland waters receive about  $19 \times 10^{14}$  g C yr<sup>-1</sup> from the  
775 terrestrial landscape, of which about  $8 \times 10^{14}$  g C yr<sup>-1</sup> are returned to the atmosphere (Cole et al.,  
776 2007). Globally the riverine input from land to ocean of organic carbon is estimated to be  
777 between  $4.5 \times 10^{14}$  g C yr<sup>-1</sup> and  $9.0 \times 10^{14}$  g C yr<sup>-1</sup>, which is at least the same amount of carbon that  
778 is taken up by the oceans from the atmosphere (Bauer et al., 2013; Cole et al., 2007).

779 The annual export of freshwater from the Amazon river of about 6,300 km<sup>3</sup> to the Atlantic Ocean  
780 (Gaillardet et al., 1997) is accompanied by  $40 \times 10^{12}$  g of organic carbon, which represents 8-10%  
781 of the global organic carbon transported to oceans by rivers (Moreira-Turcq et al., 2003; Richey  
782 et al., 1990). Our estimates of the discharge of organic carbon to the Atlantic are larger. As  
783 already shown in other studies (Gerten et al., 2004; Langerwisch et al., 2013) LPJmL is able to  
784 reproduce observed discharge patterns. As already discussed (4.1.) small deviations between  
785 observed and simulated discharge or even a small shift in seasonality (1-2 months) can lead to a  
786 comparably large difference in discharged carbon, because the combination of the simulated  
787 concentration and amount of water discharged determines the amount of discharged carbon to



788 the Atlantic Ocean. In addition to that, the overestimation of export to the ocean is partly caused  
789 by up and downscaling of observation data. Our estimates of riverine TOC export represents  
790 about 1-2% of the net basin primary production (Moreira-Turcq et al., 2003) is in agreement with  
791 the results of our study (1% during reference period). Our results suggest that this proportion will  
792 change by -10% to +10% due to climate change. The continuous input of organic matter into the  
793 ocean fundamentally impacts the primary production of the Atlantic Ocean off the coast of South  
794 America (Körtzinger, 2003; Cooley and Yager, 2006; Cooley et al., 2007; Subramaniam et al.,  
795 2008). In addition to organic carbon, also nutrients, which are only marginally taken up by the  
796 low primary production within the river, are exported to the ocean fuelling oceanic heterotrophy  
797 and primary production, respectively.

798 The inclusion of inundation and the corresponding transport and conversion of organic material  
799 leads to an increase in outgassed carbon of more than 3%, which equals to about  
800  $14.5 \times 10^{12}$  g month<sup>-1</sup>. This amount increases to up to  $18.3 \times 10^{12}$  g month<sup>-1</sup> due to climate change.  
801 The proportion of outgassed carbon from water bodies is an indicator for the importance of the  
802 riverine system to carbon dynamics of the entire basin. It emphasizes the importance of the  
803 implementation of floodplain systems to vegetation models, especially for Amazonia. Including  
804 inundation and export of organic material to vegetation models seems to be of minor importance,  
805 because the carbon is only transported but its quantity does not change. This is only partly true  
806 since the organic material is no longer available on site (e.g. as fertilizer) but is removed from  
807 one location and finally from the entire system. Including this export leads to a more realistic  
808 estimation of carbon fluxes, and ignoring this constant drain of carbon from the Amazon basin,  
809 would therefore overestimate the general ability of Amazonia to sequester carbon. Only coupled  
810 models can cover the interconnection between land and river, which might be important to  
811 identify non-linear feedbacks on climate change (Bauer et al., 2013). Our approach serves as a  
812 basis for simulating carbon modification and transport from the terrestrial biosphere through  
813 river systems to the oceans and establishes the link between continental and oceanic systems on a  
814 continental scale.

## 815 **5 Summary**

816 We aimed to develop a coupled terrestrial-riverine model to understand the effects of climate  
817 change on carbon fluxes in such a coupled system. We applied the model to the Amazon basin  
818 which could serve as a blueprint for studying other systems where such a tight coupling of the  
819 terrestrial and riverine part appears. With our approach we were able to estimate potential  
820 changes in exported and riverine carbon pools and fluxes from present until 2100 for the  
821 Amazon basin. We showed that the export of carbon to the Atlantic Ocean could increase  
822 slightly by about 1%, while the export to the atmosphere could increase by about 40%. To  
823 estimate these changes we coupled the newly developed riverine carbon model RivCM to the  
824 well-established vegetation and hydrology model LPJmL. These large export fluxes are

825 accompanied with changes in terrestrial organic carbon and riverine organic and inorganic  
826 carbon. Our results suggest that coupling terrestrial with riverine carbon is an important step  
827 towards a better understanding of the effects of climate change on large scale catchment carbon  
828 dynamics.

829

830 *Author contributions.* Model development: FL, BT, WC. Data analysis: FL, AR, KT. Writing the  
831 article: FL, AR, AW, BT, KT.

832 *Acknowledgements.* We thank “Pakt für Forschung der Leibniz-Gemeinschaft” for funding the  
833 TRACES project for FL. AR was funded by FP7 AMAZALERT (ProjectID 282664) and  
834 Helmholtz Alliance ‘Remote Sensing and Earth System Dynamics’. We also thank Susanne  
835 Rolinski and Dieter Gerten for discussing the hydrological aspects. We thank Alice Boit for  
836 fruitful comments on the manuscript. Additionally we thank our LPJmL and ECOSTAB  
837 colleagues at PIK for fruitful comments on the design of the study and the manuscript. We also  
838 thank the anonymous reviewers whose comments and suggestions largely improved the  
839 manuscript.

840

## 841 **6 References**

842 Abril, G., Martinez, J.-M., Artigas, L. F., Moreira-Turcq, P., Benedetti, M. F., Vidal, L.,  
843 Meziane, T., Kim, J.-H., Bernardes, M. C., Savoye, N., Deborde, J., Souza, E. L., Albéric, P.,  
844 Landim de Souza, M. F. and Roland, F.: Amazon River carbon dioxide outgassing fuelled by  
845 wetlands, *Nature*, 505(7483), 395–398, doi:10.1038/nature12797, 2014.

846 Allison, M. A., Nittrouer, C. A. and Kineke, G. C.: Seasonal sediment storage on mudflats  
847 adjacent to the Amazon river, *Mar. Geol.*, 125(3–4), 303–328, 1995.

848 Amon, R. M. W. and Benner, R.: Photochemical and microbial consumption of dissolved  
849 organic carbon and dissolved oxygen in the Amazon River system, *Geochim. Cosmochim. Acta*,  
850 60(10), 1783–1792, 1996.

851 Anderson, J. T., Nuttle, T., Saldaña Rojas, J. S., Pendergast, T. H. and Flecker, A. S.: Extremely  
852 long-distance seed dispersal by an overfished Amazonian frugivore, *Proc. R. Soc. B Biol. Sci.*,  
853 278, 3329–3335, doi:10.1098/rspb.2011.0155, 2011.

854 Aufdenkampe, A. K., Mayorga, E., Hedges, J. I., Llerena, C., Quay, P. D., Gudeman, J.,  
855 Krusche, A. V. and Richey, J. E.: Organic matter in the Peruvian headwaters of the Amazon:  
856 Compositional evolution from the Andes to the lowland Amazon mainstem, *Org. Geochem.*,  
857 38(3), 337–364, doi:10.1016/j.orggeochem.2006.06.003, 2007.

- 858 Bauer, D. F.: Constructing confidence sets using rank statistics, *J. Am. Stat. Assoc.*, 67(339),  
859 687–690, 1972.
- 860 Bauer, J. E., Cai, W.-J., Raymond, P. A., Bianchi, T. S., Hopkinson, C. S. and Regnier, P. A. G.:  
861 The changing carbon cycle of the coastal ocean, *Nature*, 504(7478), 61–70,  
862 doi:10.1038/nature12857, 2013.
- 863 Belger, L., Forsberg, B. R. and Melack, J. M.: Carbon dioxide and methane emissions from  
864 interfluvial wetlands in the upper Negro River basin, Brazil, *Biogeochemistry*, 105, 171–183,  
865 doi:10.1007/s10533-010-9536-0, 2011.
- 866 Benner, R., Opsahl, S., Chin-Leo, G., Richey, J. E. and Forsberg, B. R.: Bacterial carbon  
867 metabolism in the Amazon River system, *Limnol. Oceanogr.*, 40(7), 1262–1270, 1995.
- 868 Biemans, H., Hutjes, R. W. A., Kabat, P., Strengers, B. J., Gerten, D. and Rost, S.: Effects of  
869 precipitation uncertainty on discharge calculations for main river basins, *J. Hydrometeorol.*,  
870 10(4), 1011–1025, doi:10.1175/2008jhm1067.1, 2009.
- 871 Bogan, T., Mohseni, O. and Stefan, H. G.: Stream temperature-equilibrium temperature  
872 relationship, *Water Resour. Res.*, 39(9), doi:1245 10.1029/2003wr002034, 2003.
- 873 Bondeau, A., Smith, P. C., Zaehle, S., Schaphoff, S., Lucht, W., Cramer, W., Gerten, D., Lotze-  
874 Campen, H., Müller, C., Reichstein, M. and Smith, B.: Modelling the role of agriculture for the  
875 20th century global terrestrial carbon balance, *Glob. Change Biol.*, 13(3), 679–706,  
876 doi:10.1111/j.1365-2486.2006.01305.x, 2007.
- 877 Bustillo, V., Victoria, R. L., de Moura, J. M. S., Victoria, D. D., Andrade Toledo, A. M. and  
878 Colicchio, E.: Biogeochemistry of carbon in the Amazonian floodplains over a 2000-km reach:  
879 Insights from a process-Based model, *Earth Interact.*, 15(4), 1–29, doi:10.1175/2010EI338.1,  
880 2011.
- 881 Coe, M. T., Latrubesse, E. M., Ferreira, M. E. and Amsler, M. L.: The effects of deforestation  
882 and climate variability on the streamflow of the Araguaia River, Brazil, *Biogeochemistry*,  
883 105(1–3), 119–131, doi:10.1007/s10533-011-9582-2, 2011.
- 884 Cole, J. J. and Caraco, N. F.: Carbon in catchments: connecting terrestrial carbon losses with  
885 aquatic metabolism, *Mar. Freshw. Res.*, 52(1), 101–110, 2001.
- 886 Cole, J. J., Pace, M. L., Carpenter, S. R. and Kitchell, J. F.: Persistence of net heterotrophy in  
887 lakes during nutrient addition and food web manipulations, *Limnol. Oceanogr.*, 45(8), 1718–  
888 1730, 2000.
- 889 Cole, J. J., Prairie, Y. T., Caraco, N. F., McDowell, W. H., Tranvik, L. J., Striegl, R. G., Duarte,  
890 C. M., Kortelainen, P., Downing, J. A., Middelburg, J. J. and Melack, J.: Plumbing the global  
891 carbon cycle: Integrating inland waters into the terrestrial carbon budget, *Ecosystems*, 10(1),  
892 171–184, doi:10.1007/s10021-006-9013-8, 2007.

- 893 Collatz, G. J., Ribas-Carbo, M. and Berry, J. A.: Coupled photosynthesis-stomatal conductance  
894 model for leaves of C4 plants, *Funct. Plant Biol.*, 19(5), 519–538, doi:10.1071/PP9920519, 1992.
- 895 Cooley, S. R. and Yager, P. L.: Physical and biological contributions to the western tropical  
896 North Atlantic Ocean carbon sink formed by the Amazon River plume, *J. Geophys. Res.-Oceans*,  
897 111(C08018), doi:10.1029/2005JC002954, 2006.
- 898 Cooley, S. R., Coles, V. J., Subramaniam, A. and Yager, P. L.: Seasonal variations in the  
899 Amazon plume-related atmospheric carbon sink, *Glob. Biogeochem. Cycles*, 21(3),  
900 doi:10.1029/2006GB002831, 2007.
- 901 Cramer, W., Bondeau, A., Woodward, F. I., Prentice, I. C., Betts, R. A., Brovkin, V., Cox, P. M.,  
902 Fisher, V., Foley, J. A., Friend, A. D., Kucharik, C., Lomas, M. R., Ramankutty, N., Sitch, S.,  
903 Smith, B., White, A. and Young-Molling, C.: Global response of terrestrial ecosystem structure  
904 and function to CO<sub>2</sub> and climate change: results from six dynamic global vegetation models,  
905 *Glob. Change Biol.*, 7(4), 357–373, 2001.
- 906 Devol, A. H., Quay, P. D., Richey, J. E. and Martinelli, L. A.: The role of gas-exchange in the  
907 inorganic carbon, oxygen, and Rn-222 budgets of the Amazon river, *Limnol. Oceanogr.*, 32(1),  
908 235–248, 1987.
- 909 Devol, A. H., Forsberg, B. R., Richey, J. E. and Pimentel, T. P.: Seasonal variation in chemical  
910 distributions in the Amazon (Solimões) river: A multiyear time series, *Glob. Biogeochem.*  
911 *Cycles*, 9(3), 307–328, 1995.
- 912 Diegues, A. C. S.: An inventory of Brazilian wetlands, Union Internationale pour la  
913 Conservation de la Nature et de ses Ressources, Switzerland, Gland, Switzerland., 1994.
- 914 Druffel, E. R. M., Bauer, J. E. and Griffin, S.: Input of particulate organic and dissolved  
915 inorganic carbon from the Amazon to the Atlantic Ocean, *Geochem. Geophys. Geosystems*, 6,  
916 Q03009, doi:10.1029/2004GC000842, 2005.
- 917 Ertel, J. R., Hedges, J. I., Devol, A. H., Richey, J. E. and Ribeiro, M. D. G.: Dissolved humic  
918 substances of the Amazon river system, *Limnol. Oceanogr.*, 31(4), 739–754, 1986.
- 919 Fader, M., Rost, S., Müller, C., Bondeau, A. and Gerten, D.: Virtual water content of temperate  
920 cereals and maize: Present and potential future patterns, *J. Hydrol.*, 384(3–4), 218–231,  
921 doi:10.1016/j.jhydrol.2009.12.011, 2010.
- 922 Farquhar, G. D., van Caemmerer, S. and Berry, J. A.: A biochemical model of photosynthetic  
923 CO<sub>2</sub> assimilation in leaves of C3 species, *Planta*, 149, 78–90, 1980.
- 924 Fearnside, P. M.: Are climate change impacts already affecting tropical forest biomass?, *Glob.*  
925 *Environ. Change-Hum. Policy Dimens.*, 14(4), 299–302, doi:10.1016/j.gloenvcha.2004.02.001,  
926 2004.

- 927 Furch, K. and Junk, W. J.: The chemical composition, food value, and decomposition of  
 928 herbaceous plants, leaves, and leaf litter of floodplain forests, in *The Central Amazon*  
 929 *Floodplain*, edited by W. J. Junk, pp. 187–205, Springer, Berlin, Germany., 1997.
- 930 Gaillardet, J., Dupré, B., Allègre, C. J. and Négrel, P.: Chemical and physical denudation in the  
 931 Amazon River basin, *Chem. Geol.*, 142(3–4), 141–173, 1997.
- 932 Gerten, D., Schaphoff, S., Haberlandt, U., Lucht, W. and Sitch, S.: Terrestrial vegetation and  
 933 water balance - hydrological evaluation of a dynamic global vegetation model, *J. Hydrol.*,  
 934 286(1–4), 249–270, doi:10.1016/j.jhydrol.2003.09.029, 2004.
- 935 Gerten, D., Rost, S., von Bloh, W. and Lucht, W.: Causes of change in 20th century global river  
 936 discharge, *Geophys. Res. Lett.*, 35(20), doi:L20405 10.1029/2008gl035258, 2008.
- 937 Gordon, W. S., Famiglietti, J. S., Fowler, N. L., Kittel, T. G. F. and Hibbard, K. A.: Validation of  
 938 simulated runoff from six terrestrial ecosystem models: results from VEMAP, *Ecol. Appl.*, 14(2),  
 939 527–545, doi:10.1890/02-5287, 2004.
- 940 Goulding, M., Barthem, R. and Ferreira, E.: *The Smithsonian Atlas of the Amazon*, Smithsonian,  
 941 Washington and London., 2003.
- 942 Gumpenberger, M., Vohland, K., Heyder, U., Poulter, B., Macey, K., Rammig, A., Popp, A. and  
 943 Cramer, W.: Predicting pan-tropical climate change induced forest stock gains and losses—  
 944 implications for REDD, *Environ. Res. Lett.*, 5(1), 14013, doi:10.1088/1748-9326/5/1/014013,  
 945 2010.
- 946 Hamilton, S. K., Sippel, S. J., Calheiros, D. F. and Melack, J. M.: An anoxic event and other  
 947 biogeochemical effects of the Pantanal wetland on the Paraguay River, *Limnol. Oceanogr.*,  
 948 42(2), 257–272, 1997.
- 949 Hedges, J. I., Cowie, G. L., Richey, J. E., Quay, P. D., Benner, R., Strom, M. and Forsberg, B.  
 950 R.: Origins and processing of organic matter in the Amazon river as indicated by carbohydrates  
 951 and amino acids, *Limnol. Oceanogr.*, 39(4), 743–761, 1994.
- 952 Hedges, J. I., Mayorga, E., Tsamakis, E., McClain, M. E., Aufdenkampe, A., Quay, P., Richey, J.  
 953 E., Benner, R., Opsahl, S., Black, B., Pimentel, T., Quintanilla, J. and Maurice, L.: Organic  
 954 matter in Bolivian tributaries of the Amazon River: A comparison to the lower mainstream,  
 955 *Limnol. Oceanogr.*, 45(7), 1449–1466, 2000.
- 956 Horn, M. H., Correa, S. B., Parolin, P., Pollux, B. J. A., Anderson, J. T., Lucas, C., Widmann, P.,  
 957 Tjiu, A., Galetti, M. and Goulding, M.: Seed dispersal by fishes in tropical and temperate fresh  
 958 waters: The growing evidence, *Acta Oecologica*, 37, 561–577, doi:10.1016/j.actao.2011.06.004,  
 959 2011.
- 960 Huntingford, C., Zelazowski, P., Galbraith, D., Mercado, L. M., Sitch, S., Fisher, R., Lomas, M.,  
 961 Walker, A. P., Jones, C. D., Booth, B. B. B., Malhi, Y., Hemming, D., Kay, G., Good, P., Lewis,  
 962 S. L., Phillips, O. L., Atkin, O. K., Lloyd, J., Gloor, E., Zaragoza-Castells, J., Meir, P., Betts, R.,

- 963 Harris, P. P., Nobre, C., Marengo, J. and Cox, P. M.: Simulated resilience of tropical rainforests  
964 to CO<sub>2</sub>-induced climate change, *Nat. Geosci.*, 6(4), 268–273, doi:10.1038/ngeo1741, 2013.
- 965 Irion, G.: Die Entwicklung des zentral- und oberamazonischen Tieflands im Spät-Pleistozön und  
966 im Holozän, *Amazoniana*, 6(1), 67–79, 1976.
- 967 Irmiler, U.: Litterfall and nitrogen turnover in an Amazonian blackwater inundation forest, *Plant  
968 Soil*, 67(1–3), 355–358, 1982.
- 969 Johnson, M. S., Lehmann, J., Selva, E. C., Abdo, M., Riha, S. and Couto, E. G.: Organic carbon  
970 fluxes within and streamwater exports from headwater catchments in the southern Amazon,  
971 *Hydrol. Process.*, 20(12), 2599–2614, 2006.
- 972 Junk, W. J.: The Amazon floodplain - A sink or source for organic carbon?, *Mitteilungen Geol.-  
973 Paläontol. Inst. Univ. Hambg.*, 58, 267–283, 1985.
- 974 Junk, W. J. and Piedade, M. T. F.: Plant life in the floodplain with special reference to  
975 herbaceous plants, in *The Central Amazon Floodplain*, edited by W. J. Junk, pp. 147–185,  
976 Springer, Berlin, Germany., 1997.
- 977 Junk, W. J. and Wantzen, K. M.: The flood pulse concept: New aspects, approaches and  
978 applications - An update, in *Proceedings of the Second International Symposium on the  
979 Management of large Rivers for Fisheries*, edited by R. L. Welcomme and T. Petr, pp. 117–140.,  
980 2004.
- 981 Jupp, T. E., Cox, P. M., Rammig, A., Thonicke, K., Lucht, W. and Cramer, W.: Development of  
982 probability density functions for future South American rainfall, *New Phytol.*, 187, 682–693,  
983 doi:10.1111/j.1469-8137.2010.03368.x, 2010.
- 984 Keeling, C. D. and Whorf, T. P.: Atmospheric CO<sub>2</sub> records from sites in the SIO air sampling  
985 network, in *Trends. A Compendium of Data on Global Change, Carbon Dioxide Inf. Anal. Cent.*,  
986 Oak Ridge Natl. Lab., US Dep. of Energy, Oak Ridge, Tenn., [online] Available from:  
987 <http://cdiac.ornl.gov/trends/co2/sio-keel.html> (Accessed 11 October 2008), 2003.
- 988 Körtzinger, A.: A significant CO<sub>2</sub> sink in the tropical Atlantic Ocean associated with the Amazon  
989 River plume, *Geophys. Res. Lett.*, 30(24), doi:10.1029/2003GL018841, 2003.
- 990 Lampert, W. and Sommer, U.: *Limnoökologie*, 2. neu bearbeitete Auflage., Thieme, Stuttgart.,  
991 1999.
- 992 Langerwisch, F., Rost, S., Gerten, D., Poulter, B., Rammig, A. and Cramer, W.: Potential effects  
993 of climate change on inundation patterns in the Amazon Basin, *Hydrol. Earth Syst. Sci.*, 17(6),  
994 2247–2262, doi:10.5194/hess-17-2247-2013, 2013.
- 995 Lauerwald, R., Laruelle, G. G., Hartmann, J., Ciais, P. and Regnier, P. A. G.: Spatial patterns in  
996 CO<sub>2</sub> evasion from the global river network, *Glob. Biogeochem. Cycles*, 29(5), 534–554,  
997 doi:10.1002/2014GB004941, 2015.

- 998 Lehner, B. and Döll, P.: Development and validation of a global database of lakes, reservoirs and  
999 wetlands, *J. Hydrol.*, 296(1–4), 1–22, doi:10.1016/j.jhydrol.2004.03.028, 2004.
- 1000 Lewin-Koh, N. J. and Bivand, R.: maptools: Tools for reading and handling spatial objects. R  
1001 package version 0.8-7., 2011.
- 1002 Lloyd, J. and Taylor, J. A.: On the temperature-dependence of soil respiration, *Funct. Ecol.*, 8(3),  
1003 315–323, 1994.
- 1004 Martius, C.: Decomposition of Wood, in *The Central Amazon Floodplain*, edited by W. J. Junk,  
1005 pp. 267–276, Springer, Berlin, Germany., 1997.
- 1006 Mayorga, E., Aufdenkampe, A. K., Masiello, C. A., Krusche, A. V., Hedges, J. I., Quay, P. D.,  
1007 Richey, J. E. and Brown, T. A.: Young organic matter as a source of carbon dioxide outgassing  
1008 from Amazonian rivers, *Nature*, 436(7050), 538–541, doi:10.1038/nature03880, 2005.
- 1009 McClain, M. E. and Elsenbeer, H.: Terrestrial inputs to Amazon streams and internal  
1010 biogeochemical processing, in *The Biogeochemistry of the Amazon Basin*, edited by M. E.  
1011 McClain, R. L. Victoria, and J. E. Richey, pp. 185–208, Oxford University Press, New York.,  
1012 2001.
- 1013 Meehl, G. A., Stocker, T. F., Collins, W. D., Friedlingstein, P., Gaye, A. T., Gregory, J. M.,  
1014 Kitoh, A., Knutti, R., Murphy, J. M., Noda, A., Raper, S. C. B., Watterson, I. G., Weaver, A. J.  
1015 and Zhao, Z.-C.: Global climate projections, in *Climate Change 2007: The Physical Science  
1016 Basis. Contribution of Working Group I to the Fourth Assessment Report of the  
1017 Intergovernmental Panel on Climate Change*, edited by S. Solomon, D. Qin, M. Manning, Z.  
1018 Chen, M. Marquis, K. B. Averyt, M. Tignor, and H. L. Miller, Cambridge University Press,  
1019 Cambridge, UK and New York, NY, USA., 2007.
- 1020 Melack, J. M. and Fisher, T. R.: Diel oxygen variations and their ecological implications in  
1021 Amazon floodplain lakes, *Arch. Fuer Hydrobiol.*, 98(4), 422–442, 1983.
- 1022 Melack, J. M. and Forsberg, B.: Biogeochemistry of Amazon floodplain lakes and associated  
1023 wetlands, in *The Biogeochemistry of the Amazon Basin and its Role in a Changing World*, pp.  
1024 235–276, Oxford University Press, Eds. McClain, M. E.; Victoria, R. L.; Richey, J. E., 2001.
- 1025 Melack, J. M., Hess, L. L., Gastil, M., Forsberg, B. R., Hamilton, S. K., Lima, I. B. T. and Novo,  
1026 E. M. L. .: Regionalization of methane emissions in the Amazon Basin with microwave remote  
1027 sensing, *Glob. Change Biol.*, 10(5), 530–544, doi:10.1111/j.1529-8817.2003.00763.x, 2004.
- 1028 Melack, J. M., Novo, E. M. L. M., Forsberg, B. R., Piedade, M. T. F. and L., M.: Floodplain  
1029 ecosystem processes, in *Amazonia and Global Change*, edited by M. Keller, M. Bustamante, J.  
1030 Gash, and P. Silva Dias, pp. 525–541, American Geophysical Union, Washington, DC., 2009.
- 1031 Mitchell, T. D. and Jones, P. D.: An improved method of constructing a database of monthly  
1032 climate observations and associated high-resolution grids, *Int. J. Climatol.*, 25(6), 693–712,  
1033 doi:10.1002/joc.1181, 2005.

- 1034 Moreira-Turcq, P., Seyler, P., Guyot, J. L. and Etcheber, H.: Exportation of organic carbon from  
 1035 the Amazon River and its main tributaries, *Hydrol. Process.*, 17(7), 1329–1344,  
 1036 doi:10.1002/hyp.1287, 2003.
- 1037 Müller-Hohenstein, K.: Die Tropenzone, in *Die Landschaftsgürtel der Erde*, pp. 51–96, B. G.  
 1038 Teubner, Stuttgart., 1981.
- 1039 Nakićenović, N., Davidson, O., Davis, G., Grübler, A., Kram, T., Lebre La Rovere, E., Metz, B.,  
 1040 Morita, T., Pepper, W., Pitcher, H., Sankovski, A., Shukla, P., Swart, R. and Dadi, Z.: IPCC  
 1041 Special report on emission scenarios, [online] Available from:  
 1042 <http://www.ipcc.ch/ipccreports/sres/emission/index.php?idp=0>, 2000.
- 1043 Nepstad, D. C., Tohver, I. M., Ray, D., Moutinho, P. and Cardinot, G.: Mortality of large trees  
 1044 and lianas following experimental drought in an Amazon forest, *Ecology*, 88(9), 2259–2269,  
 1045 doi:10.1890/06-1046.1, 2007.
- 1046 Neu, V., Neill, C. and Krusche, A. V.: Gaseous and fluvial carbon export from an Amazon forest  
 1047 watershed, *Biogeochemistry*, 105, 133–147, doi:10.1007/s10533-011-9581-3, 2011.
- 1048 Oksanen, J., Blanchet, F. G., Kindt, R., Legendre, P., O'Hara, R. B., Simpson, G. L., Solymos,  
 1049 P., Stevens, M. H. H. and Wagner, H.: vegan: Community Ecology Package. R package version  
 1050 1.17.11. [online] Available from: <http://CRAN.R-project.org/package=vegan>, 2011.
- 1051 Österle, H., Gerstengarbe, F. W. and Werner, P. C.: Homogenisierung und Aktualisierung des  
 1052 Klimadatensatzes des Climate Research Unit der Universität of East Anglia, Norwich. 6.  
 1053 Deutsche Klimatagung 2003 Potsdam, Germany, *Terra Nostra*, 2003(6), 326–329, 2003.
- 1054 Panday, P. K., Coe, M. T., Macedo, M. N., Lefebvre, P. and Castanho, A. D. de A.:  
 1055 Deforestation offsets water balance changes due to climate variability in the Xingu River in  
 1056 eastern Amazonia, *J. Hydrol.*, 523, 822–829, doi:10.1016/j.jhydrol.2015.02.018, 2015.
- 1057 Parker, A. J.: The Topographic Relative Moisture Index: An approach to soil-moisture  
 1058 assessment in mountain terrain, *Phys. Geogr.*, 3(2), 160–168, 1982.
- 1059 Poulter, B., Aragão, L., Heyder, U., Gumpenberger, M., Heinke, J., Langerwisch, F., Rammig,  
 1060 A., Thonicke, K. and Cramer, W.: Net biome production of the Amazon Basin in the 21st  
 1061 century, *Glob. Change Biol.*, 16(7), 2062–2075, doi:10.1111/j.1365-2486.2009.02064.x, 2009a.
- 1062 Poulter, B., Aragão, L., Heyder, U., Gumpenberger, M., Heinke, J., Langerwisch, F., Rammig,  
 1063 A., Thonicke, K. and Cramer, W.: Net biome production of the Amazon Basin in the 21st  
 1064 century, *Glob. Change Biol.*, 16(7), 2062–2075, doi:10.1111/j.1365-2486.2009.02064.x, 2009b.
- 1065 R Development Core Team and contributors worldwide, N. J.: stats: The R Stats Package version  
 1066 2.13.0., 2011.
- 1067 Rammig, A., Jupp, T., Thonicke, K., Tietjen, B., Heinke, J., Ostberg, S., Lucht, W., Cramer, W.  
 1068 and Cox, P.: Estimating the risk of Amazonian forest dieback, *New Phytol.*, 187(3), 694–706,  
 1069 doi:10.1111/j.1469-8137.2010.03318.x, 2010.



- 1070 Randall, D. A., Wood, R. A., Bony, S., Colman, R., Fichefet, T., Fyfe, J., Kattsov, V., Pitman,  
1071 A., Shukla, J., Srinivasan, J., Stouffer, R. J., Sumi, A. and Taylor, K. E.: Climate models and  
1072 their evaluation, in *Climate Change 2007: The Physical Science Basis. Contribution of Working*  
1073 *Group I to the Fourth Assessment Report of the Intergovernmental Panel on Climate Change*,  
1074 edited by S. Solomon, D. Qin, M. Manning, Z. Chen, M. Marquis, K. B. Averyt, M. Tignor, and  
1075 H. L. Miller, Cambridge University Press., 2007.
- 1076 Richey, J. E. and Victoria, R. L.: C, N, and P export dynamics in the Amazon river, in  
1077 *Interactions of C, N, P and S Biogeochemical Cycles and Global Change*, vol. Vol. 14, Springer  
1078 Berlin Heidelberg, Berlin, Heidelberg. [online] Available from: [http://nbn-](http://nbn-resolving.de/urn:nbn:de:1111-201111152598)  
1079 [resolving.de/urn:nbn:de:1111-201111152598](http://nbn-resolving.de/urn:nbn:de:1111-201111152598) (Accessed 4 April 2014), 1993.
- 1080 Richey, J. E., Hedges, J. I., Devol, A. H., Quay, P. D., Victoria, R., Martinelli, L. and Forsberg,  
1081 B. R.: Biogeochemistry of carbon in the Amazon River, *Limnol. Oceanogr.*, 35(2), 352–371,  
1082 1990.
- 1083 Richey, J. E., Melack, J. M., Aufdenkampe, A. K., Ballester, V. M. and Hess, L. L.: Outgassing  
1084 from Amazonian rivers and wetlands as a large tropical source of atmospheric CO<sub>2</sub>, *Nature*,  
1085 416(6881), 617–620, doi:10.1038/416617a, 2002.
- 1086 Rost, S., Gerten, D., Bondeau, A., Lucht, W., Rohwer, J. and Schaphoff, S.: Agricultural green  
1087 and blue water consumption and its influence on the global water system, *Water Resour. Res.*,  
1088 44(9), doi:W09405 10.1029/2007wr006331, 2008.
- 1089 Sander, R.: Compilation of Henry's law constants for inorganic and organic species of potential  
1090 importance in environmental chemistry, Air Chemistry Department, Max-Planck Institute of  
1091 Chemistry. [online] Available from: <http://www.mpch-mainz.mpg.de/~sander/res/henry.html>,  
1092 1999.
- 1093 Schwoerbel, J. and Brendelberger, H.: *Einführung in die Limnologie*, 9. Auflage., Elsevier,  
1094 Spektrum Akademischer Verlag, Heidelberg., 2005.
- 1095 Sioli, H.: Sedimentation im Amazonasgebiet, *Int. J. Earth Sci.*, 45(3), 608–633, 1957.
- 1096 Sitch, S., Smith, B., Prentice, I. C., Arneth, A., Bondeau, A., Cramer, W., Kaplan, J. O., Levis,  
1097 S., Lucht, W., Sykes, M. T., Thonicke, K. and Venevsky, S.: Evaluation of ecosystem dynamics,  
1098 plant geography and terrestrial carbon cycling in the LPJ dynamic global vegetation model,  
1099 *Glob. Change Biol.*, 9(2), 161–185, doi:10.1046/j.1365-2486.2003.00569.x, 2003.
- 1100 Sjögersten, S., Black, C. R., Evers, S., Hoyos-Santillan, J., Wright, E. L. and Turner, B. L.:  
1101 Tropical wetlands: A missing link in the global carbon cycle?: Carbon cycling in tropical  
1102 wetlands, *Glob. Biogeochem. Cycles*, 28, 1371–1386, doi:10.1002/2014GB004844, 2014.
- 1103 Subramaniam, A., Yager, P. L., Carpenter, E. J., Mahaffey, C., Bjorkman, K., Cooley, S.,  
1104 Kustka, A. B., Montoya, J. P., Sanudo-Wilhelmy, S. A., Shipe, R. and Capone, D. G.: Amazon  
1105 River enhances diazotrophy and carbon sequestration in the tropical North Atlantic Ocean, *Proc.*  
1106 *Natl. Acad. Sci.*, 105(30), 10460–10465, doi:10.1073/pnas.0710279105, 2008.

- 1107 Thonicke, K., Spessa, A., Prentice, I. C., Harrison, S. P., Dong, L. and Carmona-Moreno, C.:  
1108 The influence of vegetation, fire spread and fire behaviour on biomass burning and trace gas  
1109 emissions: results from a process-based model, *Biogeosciences*, 7(6), 1991–2011,  
1110 doi:10.5194/bg-7-1991-2010, 2010.
- 1111 Vannote, R. L., Minshall, G. W., Cummins, K. W., Sedell, J. R. and Cushing, C. E.: River  
1112 Continuum Concept, *Can. J. Fish. Aquat. Sci.*, 37(1), 130–137, 1980.
- 1113 Wagner, W., Scipal, K., Pathe, C., Gerten, D., Lucht, W. and Rudolf, B.: Evaluation of the  
1114 agreement between the first global remotely sensed soil moisture data with model and  
1115 precipitation data, *J. Geophys. Res.*, 108(4611), doi:10.1029/2003JD003663, 2003.
- 1116 Wantzen, K. M., Yule, C. M., Mathooko, J. M. and Pringle, C. M.: Organic matter processing in  
1117 tropical streams, in *Aquatic Ecosystems: Tropical Stream Ecology*, pp. 43–64, Elsevier Science  
1118 (USA), London., 2008.
- 1119 Waterloo, M. J., Oliveira, S. M., Drucker, D. P., Nobre, A. D., Cuartas, L. A., Hodnett, M. G.,  
1120 Langedijk, I., Jans, W. W. P., Tomasella, J., de Araújo, A. C., Pimentel, T. P. and Estrada, J. C.  
1121 M.: Export of organic carbon in run-off from an Amazonian rainforest blackwater catchment,  
1122 *Hydrol. Process.*, 20(12), 2581–2597, 2006.
- 1123 Worbes, M.: The forest ecosystem of the floodplains, in *The Central Amazon Floodplain*, edited  
1124 by W. J. Junk, pp. 223–265, Springer, Berlin, Germany., 1997.
- 1125 WWF HydroSHEDS: HydroSHEDS, [online] Available from: <http://hydrosheds.cr.usgs.gov/>  
1126 (Accessed 15 October 2007), 2007.
- 1127 Yarnell, S. M., Mount, J. F. and Larsen, E. W.: The influence of relative sediment supply on  
1128 riverine habitat heterogeneity, *Geomorphology*, 80(3–4), 310–324,  
1129 doi:10.1016/j.geomorph.2006.03.005, 2006.
- 1130 Zulkafli, Z., Buytaert, W., Manz, B., Rosas, C. V., Willems, P., Lavado-Casimiro, W., Guyot, J.-  
1131 L. and Santini, W.: Projected increases in the annual flood pulse of the Western Amazon,  
1132 *Environ. Res. Lett.*, 11(1), 14013, doi:10.1088/1748-9326/11/1/014013, 2016.
- 1133
- 1134

1135 **7 Tables**

1136

1137

**Table 1: Overview of the input used in the model.**

<i>input</i>	<i>temporal resolution</i>	<i>spatial resolution (lat/lon)</i>	<i>unit</i>	<i>source</i>
<b>static</b>				
<i>river type</i>	-	0.5° × 0.5°	-	(Diegues, 1994; Irion, 1976; Sioli, 1957)
<i>river order</i>	-	0.5° × 0.5°	-	
max. floodable area ( <i>MaxInunArea</i> )	-	0.5° × 0.5°	km <sup>2</sup>	(Langerwisch et al., 2013)
<i>rout cell</i>	-	0.5° × 0.5°	-	(Rost et al., 2008)
flow velocity ( <i>v</i> )	-	0.5° × 0.5°	m s <sup>-1</sup>	(Langerwisch et al., 2013)
soil depth ( <i>soildepth<sub>1</sub></i> , <i>soildepth<sub>2</sub></i> )	-	0.5° × 0.5°		LPJmL
<b>dynamic</b>				
atmospheric CO <sub>2</sub> ( <i>atmCO<sub>2</sub></i> )	annually	globally	ppm	SRES (see Nakićenović et al., 2000)
Temperature ( <i>T</i> )	monthly	0.5° × 0.5°	°C	IPCC (see Meehl et al., 2007)
Discharge ( <i>Mdis</i> )	monthly	0.5° × 0.5°	m <sup>3</sup> s <sup>-1</sup>	LPJmL
amount of water ( <i>Mwat</i> )	monthly	0.5° × 0.5°	m <sup>3</sup>	LPJmL
soil water content ( <i>Mswc<sub>1</sub></i> , <i>Mswc<sub>2</sub></i> )	monthly	0.5° × 0.5°	%	LPJmL
soil carbon ( <i>ASoilc</i> )	annually	0.5° × 0.5°	g m <sup>-2</sup>	LPJmL
litter carbon ( <i>ALitc</i> )	annually	0.5° × 0.5°	g m <sup>-2</sup>	LPJmL

1138

1139

1140

**Table 2 List of physical constants.**

<i>constant name</i>	<i>value</i>	<i>unit</i>	<i>source</i>
$k_H^\theta$	1.496323	$\text{g CO}_2 \text{ l}^{-1} \text{ atm}^{-1}$	(Sander, 1999)
$d\ln k_H$	2400	K	(Sander, 1999)
$T^\theta$	298.15	K	(Sander, 1999)
$ctoco2^*$	0.2729	-	

1141 \* Ratio of the atomic mass of carbon ( $12.001 \text{ g mol}^{-1}$ ) in the  $\text{CO}_2$  molecule ( $44.01 \text{ g mol}^{-1}$ ).1142 Applied to calculate the outgassed  $\text{CO}_2$ , since the model calculates the actual flux and pools of  
1143 carbon.

1144

1145

**Table 3: List of parameters.**

<i>parameter name</i>	<i>value</i>	<i>unit</i>	<i>source</i>	<i>original value</i>
<b>loss via terrestrial respiration</b>				
<i>respi<sub>litc</sub></i>	30	%	LPJmL	
<i>respi<sub>soilcfast</sub></i>	3	%	LPJmL	
<i>respi<sub>soilcslow</sub></i>	0.1	%	LPJmL	
<i>respi<sub>partsoilcfast</sub></i>	98	%	LPJmL	
<i>respi<sub>partsoilcslow</sub></i>	2	%	LPJmL	
<b>mobilization</b>				
<i>carboncorr</i>	0.65	month <sup>-1</sup>	(Worbes, 1997)	0.65 ± 0.15
<i>mobil<sub>litc</sub></i>	0.7	month <sup>-1</sup>	(Irmeler, 1982)	0.4 ± 0.1
<i>mobil<sub>soile</sub></i>	0.05	month <sup>-1</sup>	(Irmeler, 1982)	
<i>mobil<sub>p</sub></i>	0.5	-	(Johnson et al., 2006; McClain and Elsenbeer, 2001)	0.5 ± 0.25
<b>decomposition</b>				
<i>decomp</i>	0.3	month <sup>-1</sup>	(Furch and Junk, 1997)	0.3 ± 0.1
<i>decomp<sub>corr</sub></i>	0.1	month <sup>-1</sup>	(Furch and Junk, 1997)	0.1 ± 0.01
<b>respiration</b>				
<i>respi</i>	0.04	day <sup>-1</sup>	(Cole et al., 2000)	0.045 ± 0.01
<b>outgassing</b>				
<i>co2satur</i>	7.25 to 17.0	-	(Richey et al., 2002)	7.25 to 17.0

1146

1147

**Table 4: List of data used for calibration and validation.**

	<i>observation</i>	<i>simulated</i>	<i>diff</i>	<i>source</i>
<b>annually outgassed CO<sub>2</sub></b>				
basin wide [10 <sup>14</sup> g C yr <sup>-1</sup> ]	4.7	1.28	-73%	(Richey et al., 2002)
in central part <sup>a</sup> [10 <sup>14</sup> g C yr <sup>-1</sup> ]	2.1 ± 0.6	0.51	-76%	(Richey et al., 2002)
per km <sup>-2</sup> [10 <sup>8</sup> g C km <sup>-2</sup> yr <sup>-1</sup> ]	1.2 ± 0.3	0.21	-82%	(Richey et al., 2002)
	6.4 ± 6.0	0.21	-96.7%	(Abril et al., 2014)
	8.0 ± 1.8	0.21	-97.4%	(Belger et al., 2011)
	60 ± 6.8	0.21	-99.7%	(Neu et al., 2011)
<b>annually exported carbon to Atlantic Ocean (estimated at Óbidos) [10<sup>14</sup> g C yr<sup>-1</sup>]</b>				
TOC <sup>a</sup>	0.36 ± 0.1	0.64	+80%	(Richey et al., 1990), (Moreira-Turcq et al., 2003)
POC	0.12 ± 0.05	0.19	+63%	(Junk, 1985; Moreira-Turcq et al., 2003)
DOC	0.27	0.45	+67%	(Moreira-Turcq et al., 2003)
<b>annually exported carbon from sub-catchments [10<sup>12</sup> g C yr<sup>-1</sup>]</b>				
<b>POC</b>				
Vargem Grande	6.4	8.3	+30%	(Richey and Victoria, 1993)
Rio Madeira	3.2	7.4	+31%	(Richey and Victoria, 1993)
Óbidos	12.1	19.4	+20%	(Richey and Victoria, 1993)
<b>DOC</b>				
Vargem Grande	4.7	21.0	+347%	(Richey and Victoria, 1993)
Rio Negro	6.6	09.2	+39%	(Richey and Victoria, 1993)
Rio Madeira	2.6	17.5	+573%	(Richey and Victoria, 1993)
Óbidos	18.4	45.1	+91%	(Richey and Victoria, 1993)
<b>carbon concentration [10<sup>-3</sup> g C l<sup>-1</sup>]</b>				
TOC <sup>a</sup>	9.85 ± 4.5	#7.46	-24%	(Ertel et al., 1986), (Moreira-Turcq et al., 2003)
POC (average)	1.50 ± 0.5	2.16	+44%	(Moreira-Turcq et al., 2003)
Rio Negro	0.69 ± 0.16	1.85 ± 1.33	+170%	(Moreira-Turcq et al., 2003)
Rio Negro	0.37 ± 0.17	0.16	-58%	(Richey et al., 1990)
Rio Branco	0.71 ± 0.28	2.03 ± 0.67	+190%	(Moreira-Turcq et al., 2003)
Rio Solimões	1.26 ± 0.47	0.66 ± 0.61	-48%	(Moreira-Turcq et al., 2003)
Rio Madeira	1.73 ± 1.8	1.42 ± 1.39	-18%	(Moreira-Turcq et al., 2003)
Rio Madeira	2.87 ± 1.24	1.70	-41%	(Richey et al., 1990)
Rio Japura	1.88 ± 0.39	1.02	-46%	(Richey et al., 1990)
Itapeua	3.21 ± 0.52	1.80	-44%	(Richey et al., 1990)
Óbidos	2.41 ± 0.39	0.13	-87%	(Richey et al., 1990)
DOC (average)	7.35 ± 4.0	5.30	-28%	(Ertel et al., 1986; Hedges et al., 1994; Moreira-Turcq et al., 2003)
Rio Negro	11.61 ± 5.49	2.07 ± 1.42	-82%	(Moreira-Turcq et al., 2003)
Rio Negro	8.43 ± 1.20	0.38	-95%	(Richey et al., 1990)
Rio Branco	2.4	2.25 ± 0.75	-6%	(Moreira-Turcq et al., 2003)
Rio Solimões	4.26 ± 1.67	1.52 ± 1.32	-64%	(Moreira-Turcq et al., 2003)
Rio Madeira	4.31 ± 2.23	7.16 ± 5.49	+66%	(Moreira-Turcq et al., 2003)
Rio Madeira	3.49 ± 1.18	0.40	+88%	(Richey et al., 1990)

Rio Japura	3.46 ± 0.66	2.44	-29%	(Richey et al., 1990)
Itapeua	3.76 ± 0.83	3.82	+2%	(Richey et al., 1990)
Óbidos	4.03 ± 0.70	0.74	-82%	(Richey et al., 1990)
IC (average)	0.95-4.08	1.64	-70-60%	(Neu et al., 2011; Richey et al., 2002)
Vargem Grande	1.12	1.84	+64%	(Devol et al., 1987)
Rio Icó	2.07	1.78	-14%	(Devol et al., 1987)
Rio Juruá	2.71	2.67	- 2%	(Devol et al., 1987)
Jutica	1.77	1.72	- 3%	(Devol et al., 1987)
Manacapuru	1.79	1.64	- 8%	(Devol et al., 1987)
Rio Negro	1.44	1.72	+20%	(Devol et al., 1987)
Rio Madeira	2.34	1.75	-25%	(Devol et al., 1987)
Óbidos	1.98	1.69	-15%	(Devol et al., 1987)
<b>Willmott's Index of Agreement</b>				
calibration data <sup>a</sup>	before calibration	0.870	after calibration	0.893
other data		0.413		0.635
all data		0.427		0.615

1149 Comparison of observed values with results of the simulations using initial parameter setting  
1150 (before calibration) and calibrated parameter setting. Difference (*diff*) is relative difference to  
1151 observation [%]. A Willmott's Index of Agreement of 1.0 indicates full agreement. <sup>a</sup> indicates  
1152 data used for calibration.

1153

1154

1155 **Table 5: Location and characteristics of the three subregions.**

	<i>North-West corner</i>	<i>South-East corner</i>	<i>area [10<sup>3</sup>km<sup>2</sup>]</i>	<i>changes in inundation length*</i>	<i>changes in inundated area*</i>
R1	0.5°S / 78.5°W	7.0°S / 72.0°W	523.03	1 month longer	larger
R2	1.0°S / 70.0°W	5.0°S / 52.0°W	891.32	±½ month shift	heterogeneous
R3	4.5°S / 58.0°W	11.0°S / 52.0°W	523.03	½ shorter	smaller

1156 Regions are also depicted in Fig. 6A. \* Changes in inundation compared to the average of 1961-  
1157 1990, as estimated and discussed in Langerwisch et al. (2013).

1158

1159



**Table 6: Mean annual export of carbon during reference and future period.**

	<i>TOC discharge to ocean</i>		<i>outgassed carbon to atmosphere</i>							
			<i>Standard<sup>a</sup></i>				<i>NoInun<sup>b</sup></i>		<i>NoRiv<sup>c</sup></i>	
	<i>sum</i> [10 <sup>12</sup> g yr <sup>-1</sup> ]	<i>prop of NPP</i> [%]	<i>SUM</i> [10 <sup>12</sup> g yr <sup>-1</sup> ]	<i>terr.</i> [10 <sup>12</sup> g yr <sup>-1</sup> ] ([%])	<i>riv.</i> [10 <sup>12</sup> g yr <sup>-1</sup> ] ([%])	<i>prop of NPP</i> [%]	<i>sum 100% terr.</i> [10 <sup>12</sup> g yr <sup>-1</sup> ]	<i>rel. to SUM</i> [%]	<i>sum 100% terr.</i> [10 <sup>12</sup> g yr <sup>-1</sup> ]	<i>rel. to SUM</i> [%]
<b>BASIN WIDE</b>										
<b>reference period</b>										
	54.1	1.0	5271.6	5081.8 (96.4)	189.8 (3.6)	3.5	5097.6	-3.3	5266.8	-0.10
<b>future period</b>										
A1B	49.3	0.75	6469.2	6204.0 (95.9)	265.2 (4.1)	4.0	6258	-3.3	6463.2	-0.10
prop. to ref	(-8.9)		(+22.7)				(+22.8)		(+22.7)	
A2	59.1	0.87	6753.6	6463.2 (95.7)	290.4 (4.3)	4.2	6534.0	-3.2	6748.8	-0.07
prop. to ref	(+9.1)		(+28.1)				(+28.2)		(+28.1)	
B1	56.6	0.90	6380.4	6163.6 (96.1)	248.8 (3.9)	3.9	6172.8	-3.3	6375.6	-0.07
prop. to ref	(+4.6)		(+21.0)				(+21.1)		(+21.1)	
<b>MAIN STEM (R2)</b>										
<b>reference period</b>										
			784.8	745.6 (95.0)	39.2 (5.0)	4.9	753.6	-4.0	780	-0.61
<b>future period</b>										
A1B			925.2	873.4 (94.4)	51.8 (5.6)	5.7	888.0	-3.9	920.4	-0.54
prop. to ref			(+17.8)				(+17.9)		(+17.9)	
A2			960.0	903.4 (94.1)	56.6 (5.9)	6.1	921.6	-3.9	954	-0.54
prop. to ref			(+22.3)				(+22.3)		(+22.2)	
B1			930.0	880.7 (94.7)	49.3 (5.3)	5.6	892.8	-3.9	925.2	-0.53
prop. to ref			(+18.4)				(+18.5)		(+18.5)	

1161 Mean annual export of carbon in reference period (1971-2000) and future period (2070-2099),  
 1162 averaged over five climate models. Discharged carbon in [10<sup>12</sup> g yr<sup>-1</sup>], and outgassed carbon in  
 1163 [10<sup>12</sup> g month<sup>-1</sup>] from the forest (terr.) and the river (riv.). List of discharged total organic carbon  
 1164 into the Atlantic Ocean and basin wide monthly outgassed carbon produced via heterotrophic  
 1165 respiration. NPP is net primary production. Proportional differences [%] between reference and  
 1166 future period are in round brackets. Differences in total outgassed carbon between future and

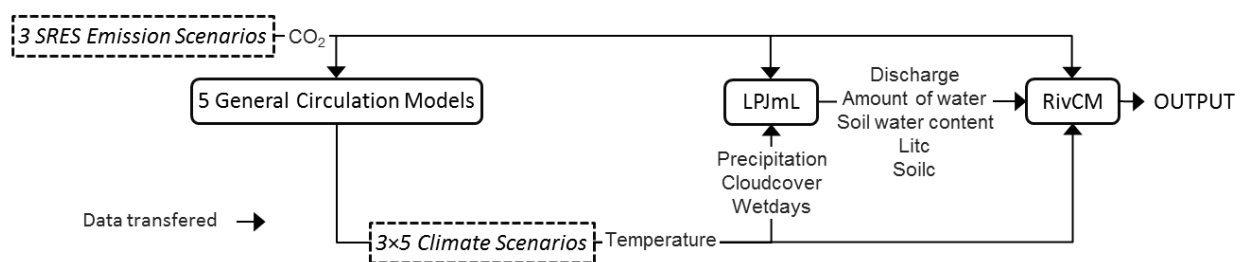
1167 reference values are in all cases highly significant (Wilcoxon Rank-Sum Test;  $p < 0.001$ ).  
1168 Negative (positive) values indicate a decrease (increase) compared to the *Standard* simulations.  
1169 <sup>a</sup>*Standard* RivCM simulations; <sup>b</sup>RivCM simulation without additional inundation (*NoInun*),  
1170 therefore no export of terrigenous organic carbon; <sup>c</sup>LPJmL calculating forest instead of river  
1171 (*NoRiv*). For details of river area calculation see Langerwisch et al. (2013).

1172

1173

1174 **8 Figures**

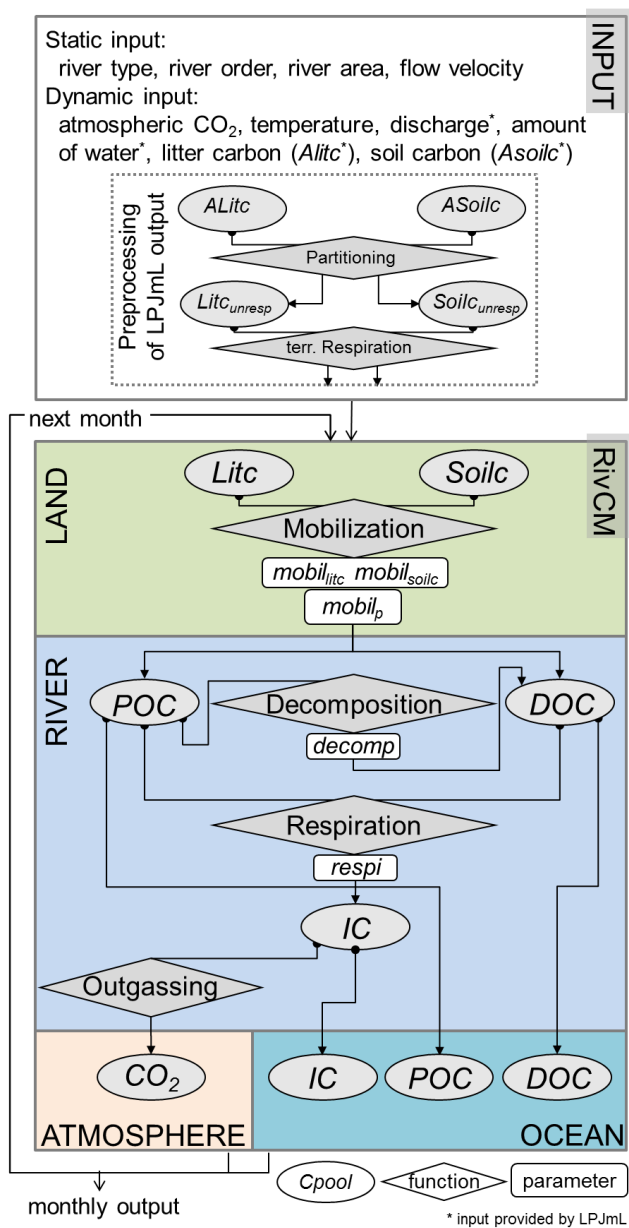
1175



1176

1177 **Figure 1.** Overview about the transfer of data between the models and scenarios.

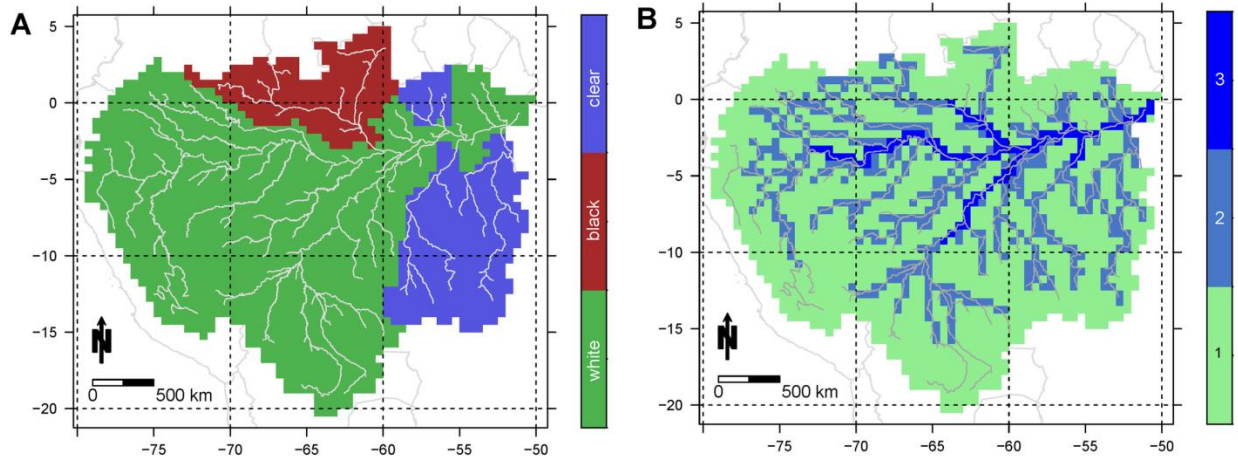
1178



1179

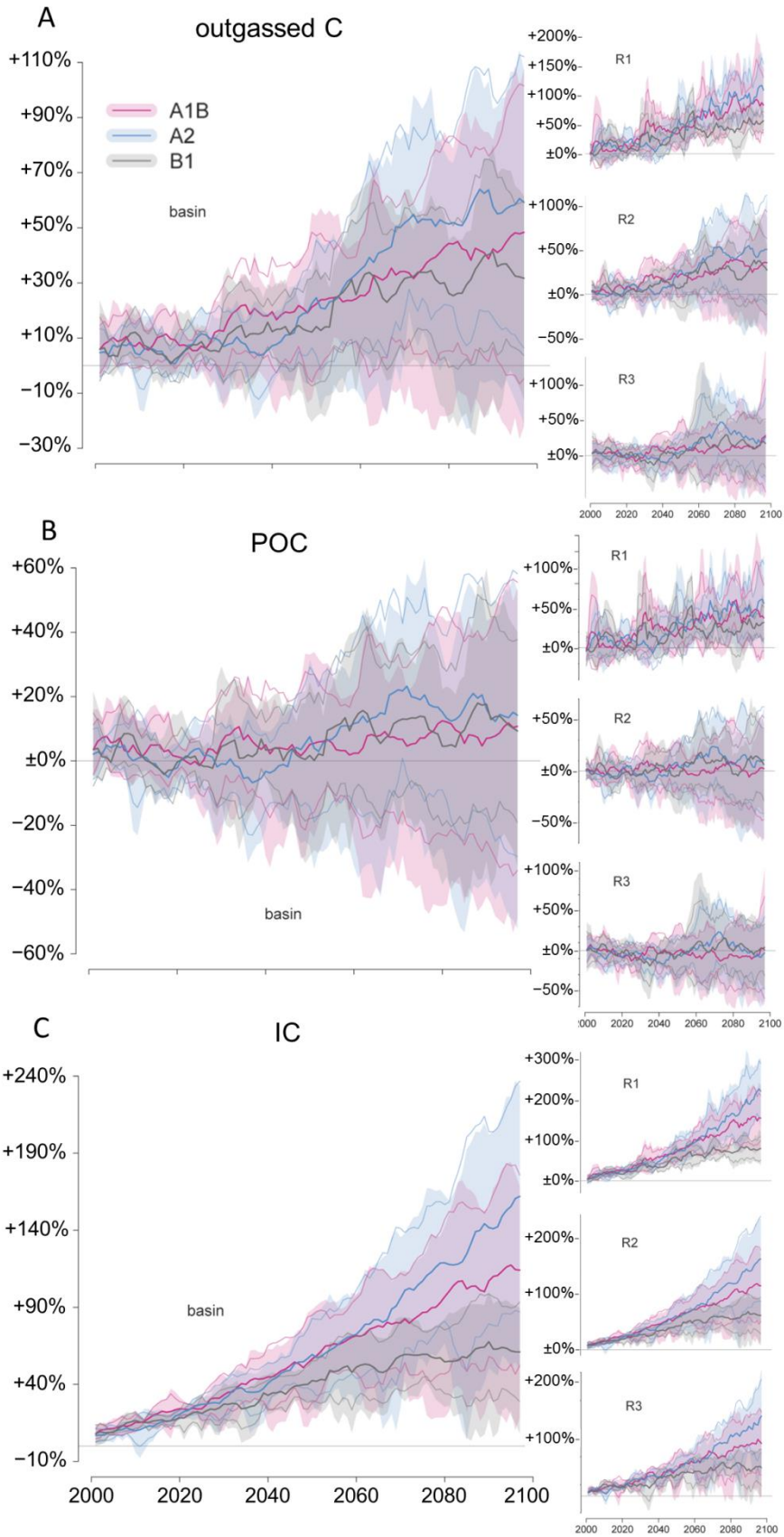
1180 **Figure 2.** Input and flow chart of RivCM. The four spatial components ‘LAND’, ‘RIVER’,  
 1181 ‘ATMOSPHERE’, and ‘OCEAN’ are connected by the exchange of carbon between different  
 1182 carbon pools (ovals), to, within, and from the river. The carbon pools are transformed through  
 1183 the most relevant processes (diamonds) with specific rates and ratios (rectangles). After the  
 1184 initialization of the input, calculations are conducted on a monthly basis. Litc = carbon in litter,  
 1185 Soilc = carbon in soil, POC = particulate organic carbon, DOC = dissolved organic carbon, IC =  
 1186 inorganic carbon.

1187

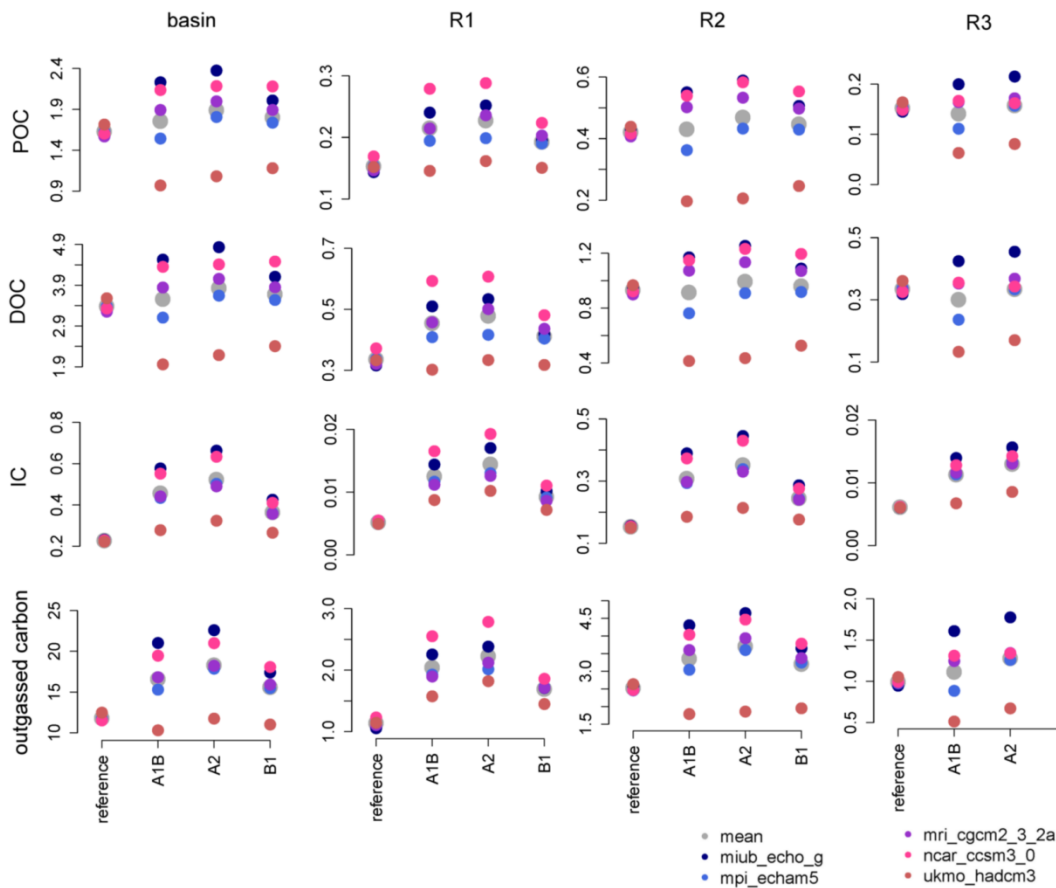


1188

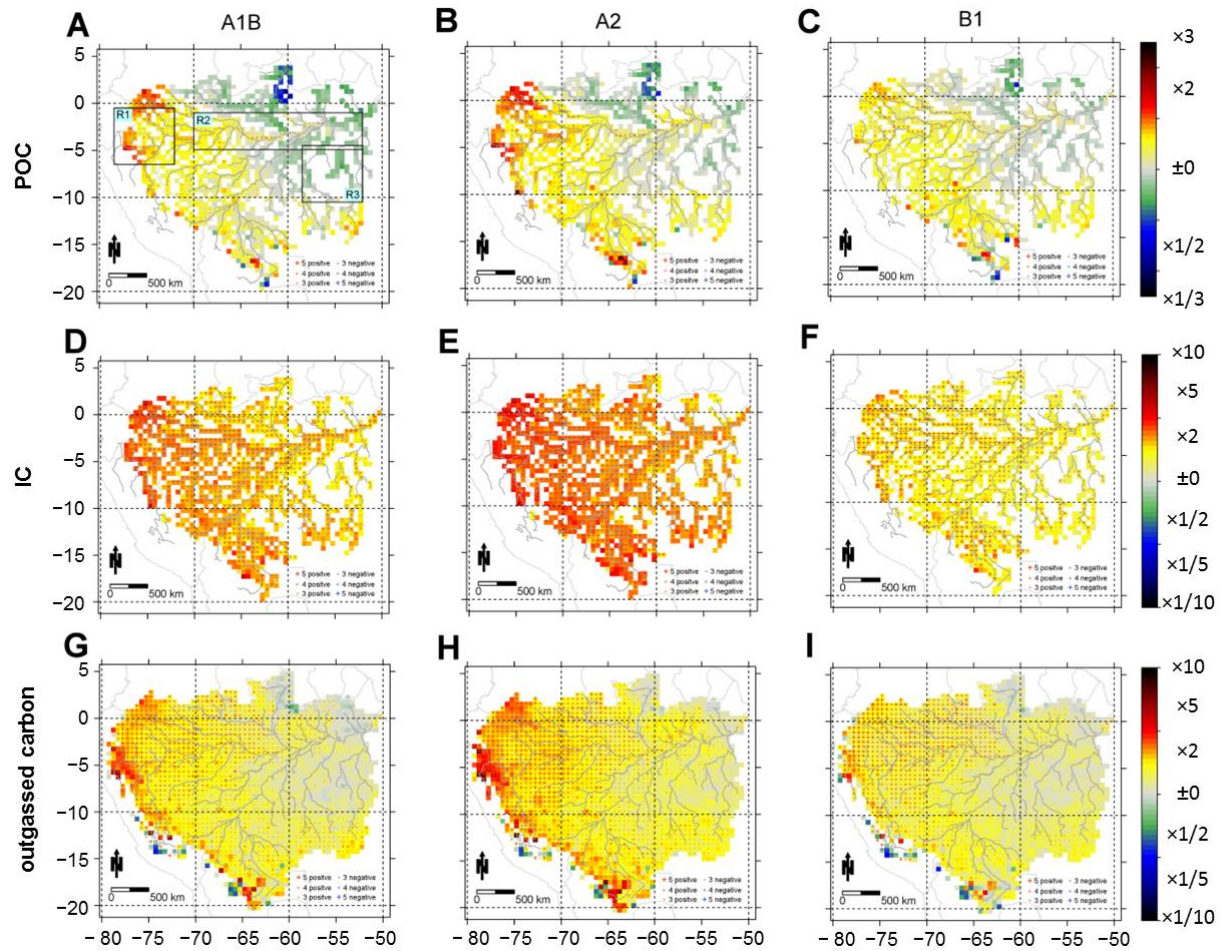
1189 **Figure 3.** River type (A) and river order (B). Cells of river order 1 (headwater) have a mean  
 1190 annual discharge of less than  $8 \times 10^3 \text{ m}^3 \text{ yr}^{-1}$ ; cells of river order 2 have a discharge between  
 1191  $8 \times 10^3$  and  $2 \times 10^5 \text{ m}^3 \text{ yr}^{-1}$ ; cells of river order 3 have a discharge higher than  $2 \times 10^5 \text{ m}^3 \text{ yr}^{-1}$ .  
 1192



1194 **Figure 4.** Temporal change in riverine carbon pools caused by climate change. (A) showing  
 1195 results for outgassed carbon, (B) for particulate organic carbon (POC) and (C) for inorganic  
 1196 carbon. Results are shown as the quotient of annual carbon amount and mean annual carbon  
 1197 amount in reference period, for the whole basin and the three subregions (R1-R3). Different  
 1198 colors represent different SRES emission scenarios. The shaded area for each scenario is spanned  
 1199 by the minimal and maximal values of all five climate models/scenarios. Bold lines represent the  
 1200 5-year-mean of the climate models/scenarios and thin lines represent mean  $\pm 1.0$  standard  
 1201 deviation. Positive values indicate an increase in outgassed CO<sub>2</sub> in the future compared to  
 1202 reference period, and negative values indicate a decrease. The horizontal line at y = 1 indicates  
 1203 no change compared to the reference period 1971-2000.  
 1204



1205 **Figure 5.** Mean annual sums of carbon pools [ $10^{12}$  g] for the whole basin and three subregions  
 1206 for the reference period (1971-2000) and the future period (2070-2099, SRES A1B, A2 and B1).  
 1207 Each for five climate models/scenarios.  
 1208  
 1209



1210

1211

1212

1213

1214

1215

1216

1217

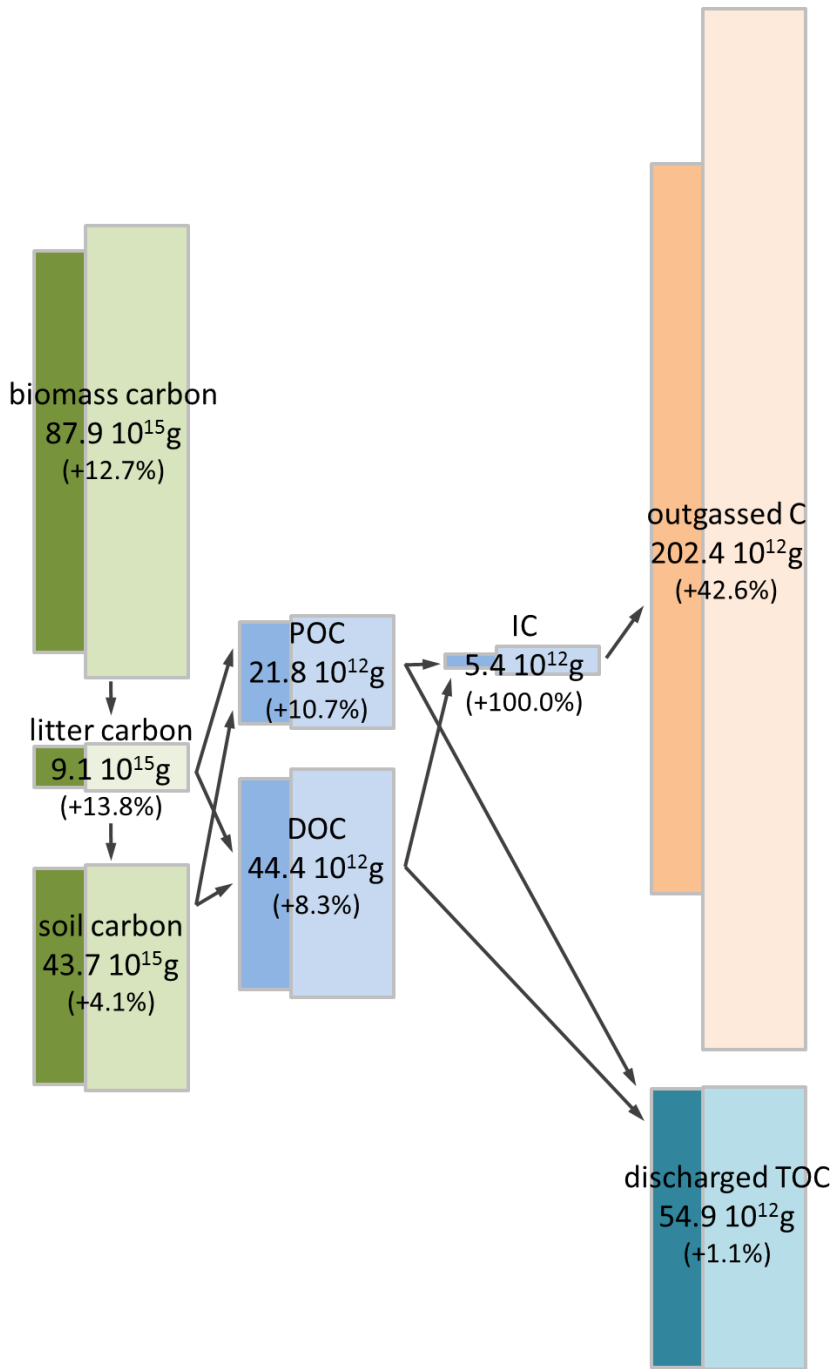
1218

1219

1220

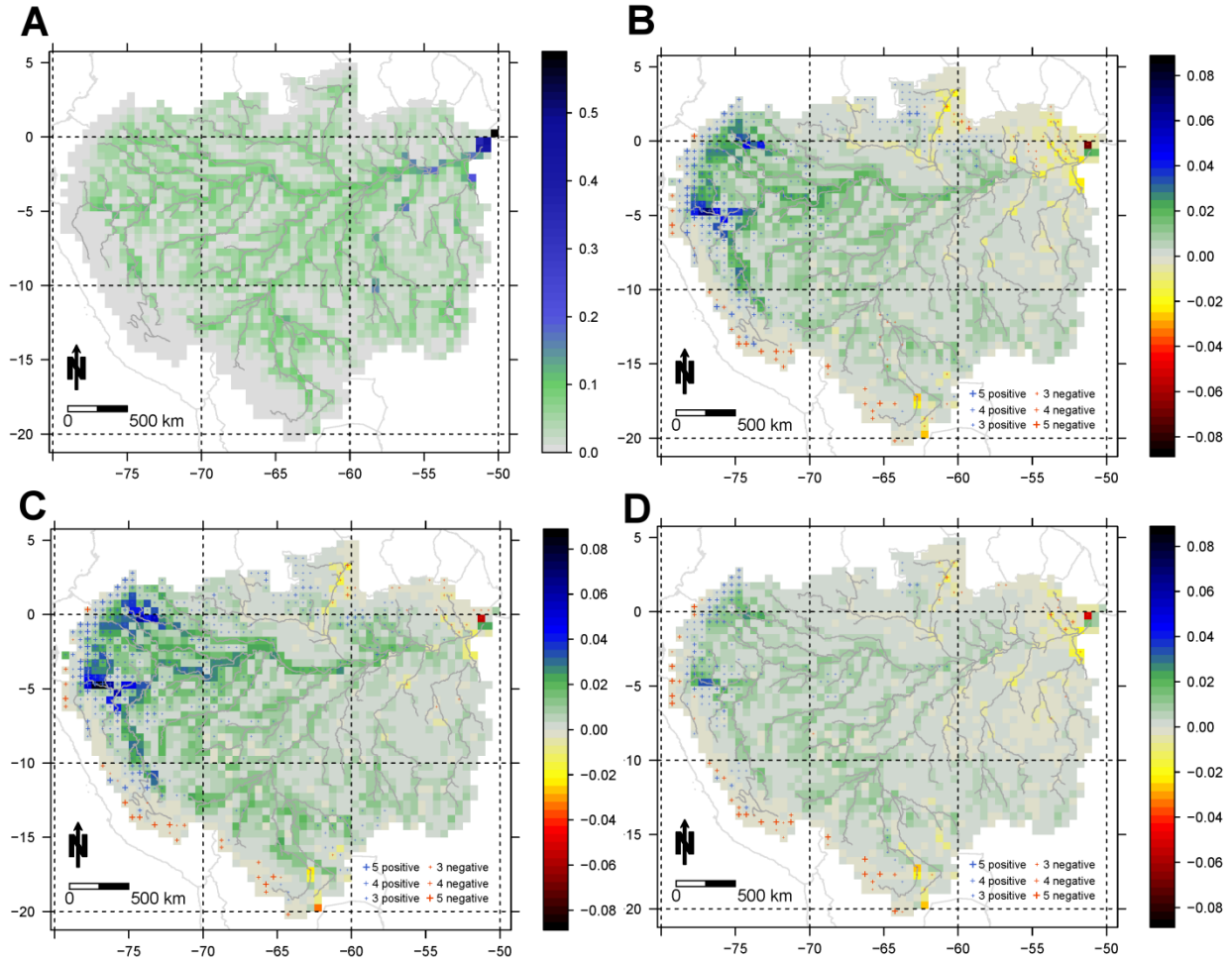
**Figure 6.** Change in riverine and outgassed carbon caused by climate change. Model mean of the relative increase and decrease of future mean and reference mean of POC (A-C) and IC (D-F) and outgassed carbon (G-I). Left hand side panels (A, D, G) show the mean of the quotient for SRES A1B emission scenario, middle panels (B, E, H) A2, right hand side (C, F, I) B1, averaged over five climate models/scenarios. Positive values (yellow and red) indicate an increase and negative values (green and blue) indicate a decrease. Additionally to the mean, the number of climate models/scenarios leading to significant trends ( $p < 0.05$ , Wilcoxon Rank-Sum Test) is indicated by crosses. In white cells the differences between future and reference values are not significant.





1221  
 1222 **Figure 7.** Averaged change in the basin carbon budget due to climate change (B). Dark boxes  
 1223 indicate the amount of carbon during the reference period, light boxes during the future period  
 1224 (average over all SRES scenarios and GCMs). Amount is given for future period with relative  
 1225 change compared to reference. Arrows indicate the direction of carbon transport.

1226



1227  
 1228  
 1229  
 1230  
 1231  
 1232  
 1233  
 1234

**Figure 8.** Proportion of outgassed carbon from the river to total outgassed carbon. Proportion of riverine outgassing to total outgassing of carbon (A) during the reference period (1971-2000) and the difference in this proportion between future (2070-2099) and reference period caused by climate change averaged over five climate models/scenarios in emission scenario A1B (B), A2 (C) and B1 (D), positive values indicate an increase and negative values indicate a decrease in the future period.